國 立 交 通 大 學

光電工程研究所

碩 士 論 文

以電漿輔助化學氣相沉積法
開發雙接面矽薄膜太陽能電池

Development of Tandem Thin-Film Silicon Solar Cells

by Plasma-Enhanced Chemical Vapor Deposition

研究生：李建亞 Chien-Ya Lee

指導教授：蔡娟娟 教授 Prof. C.C. Tsai

中華民國九十九年八月

以電漿輔助化學氣相沉積法開發雙接面矽薄膜太陽能電池

Development of Tandem Thin-Film Silicon Solar Cells by Plasma-Enhanced Chemical Vapor Deposition

研究生：李建亞　　　　　　　　　Student：Chien-Ya Li

指導教授：蔡娟娟 教授　　　　　　Advisor：Prof. C.C. Tsai

國 立 交 通 大 學

光電工程研究所

碩士論文

A Thesis

Submitted to Department of Photonics

Display Institute

College of Electrical Engineering and Computer Science

National Chiao Tung University

In partial Fulfillment of the Requirements

For the Degree of

Master

In

Electro-Optical Engineering

August 2009

Hsinchu, Taiwan, Republic of China

中華民國九十九年八月

中文摘要

在本研究中，主要目標為開發雙接面矽薄膜太陽能電池，因此從兩個方向進行研究，一個為非晶矽薄膜堆疊太陽能電池，一個為微晶矽薄膜開發再延伸到非晶矽及微晶矽堆疊薄膜太陽能電池。本研究是利用射頻電漿輔助化學氣相沉積系統來沉積非晶矽和微晶矽薄膜。

在非晶矽薄膜堆疊太陽能電池的研究中，藉由調變上層太陽能電池的吸收層厚度來達到電流匹配，此外也加入能帶漸變的應用來改善短路電流。在穿隧複合接面上，藉由調變非晶矽 n-type 層的厚度來減少此層所造成的光線吸收，另外加入微晶矽 n-type 層來改善原本由非晶矽 n-type 層和 p-type 層所造成的反向二極體。

在微晶矽薄膜開發方面，藉由調變總流率、電漿功率和氫氣稀釋比例來探討微晶矽薄膜的材料特性。微晶矽薄膜是在高壓力以及高電漿功率中成膜。在 X 射線散射儀的量測和光感應中都顯示良好的材料特性在較低的電漿功率和非晶矽轉換成微晶矽的過渡區。

Abstract

In this study, the major objective is to develop silicon based tandem solar cell. There are two directions to achieve this objective: development of a-Si:H / a-Si:H tandem solar cell and deposition and characteristic of the intrinsic μc-Si:H thin film to fabricate a-Si:H / μc-Si:H tandem solar cell. Both a-Si:H and μc-Si:H were deposited by plasma-enhanced chemical vapor deposition (PECVD) system at 27.12 MHz

In the part of a-Si:H / a-Si:H tandem solar cell, we varied the thickness of top cell to achieve current matching. Beside, the band-gap profiling is used in buffer grading to improve short-circuit current density (J_{sc}). μc-Si:H n-layer is applied in tunneling recombination junction (TRJ), it shows no reverse electric field against the built-in voltage of top and bottom cell compared with the TRJ with μc-Si:H n-layer.

In the part of intrinsic μc-Si:H thin film deposition, The effect of total flow rate, power and hydrogen dilution ratio on intrinsic μc-Si:H thin film characteristic has been studied. The μc-Si:H thin films were deposited under high pressure and high power condition. The transition region from a-Si:H to μc-Si:H shows a good material characteristic both in X-ray diffraction spectroscopy (XRD) and photosensitivity.

Acknowledgements

Content

List of Tables

List of Figures

VIII

x

Chapter 1   INTRODUCTION

1.1 Global Warming and Energy Problem

The global warming has already caused many worldwide disasters including floods, droughts, and the related problems like contagions and famine. Based on many research groups' results, such as IPCC, there is an apparent relationship between the carbon dioxide concentration and global temperature. The biggest source of carbon dioxide is the utilization of fossil fuel, especially in the energy field. Thus, in order to lower the damage to our environment, developing clean and renewable energy is one effective approach. Among various energy sources, photovoltaic (solar power) has the advantages of pollution-free during use and the lasting energy input from the sun, making photovoltaic one of the most promising clean energy method. As shown in Fig. 1-1, based on the prediction of German Advisory Council on Global Change (WBGU), solar power will be one of the highest-growing and the dominant energy resource in the future 100 years.
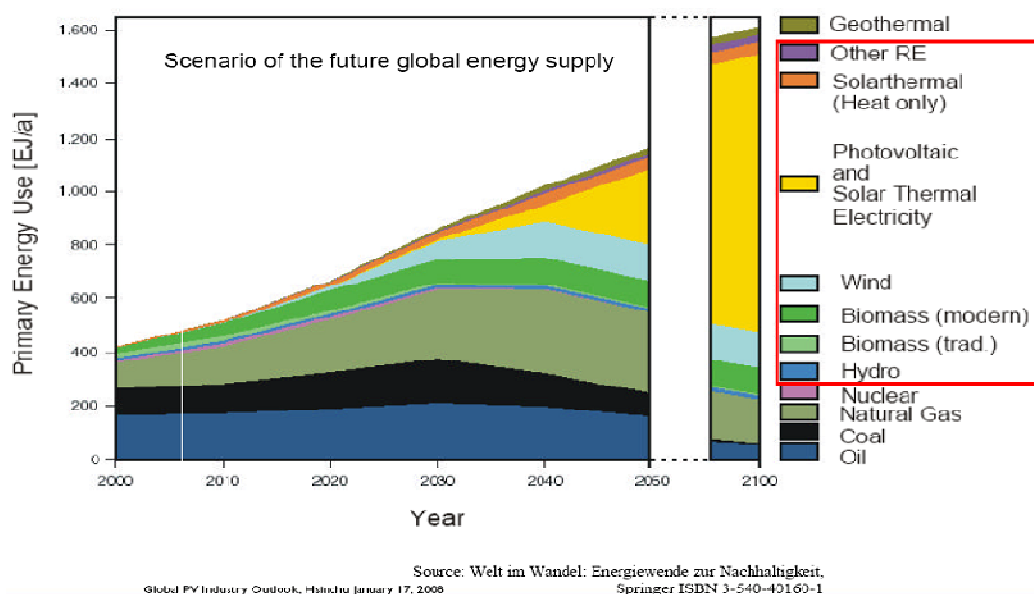
Fig. 1-1   The change in the global energy composition until 2050 / 2100

1

1.2 Introduction to Photovoltaic (PV) Technology

1.2.1 Current Development of PV Technology

There are three generations of solar cell. The first generation is silicon wafer-based solar cell, which is with higher conversion efficiency but higher costs. The second generation is thin film solar cell, which is with lower costs as well as lower conversion efficiency. The third generation is solar cell with new materials such as organic solar cell or dye-sensitized solar cell, which are still during the laboratory stage.

As shown in Fig. 1-2, the historical efficiency record from Nation Renewable Energy Laboratory (NREL) demonstrates that the efficiency of the research-cell is still being improved in various kinds of solar cell. Generally speaking, the higher conversion efficiency often accompanies with higher cost or complicated fabrication process. The goal of grid-parity can only be achieved when the cost per watt is low enough compare to current fossil fuel.
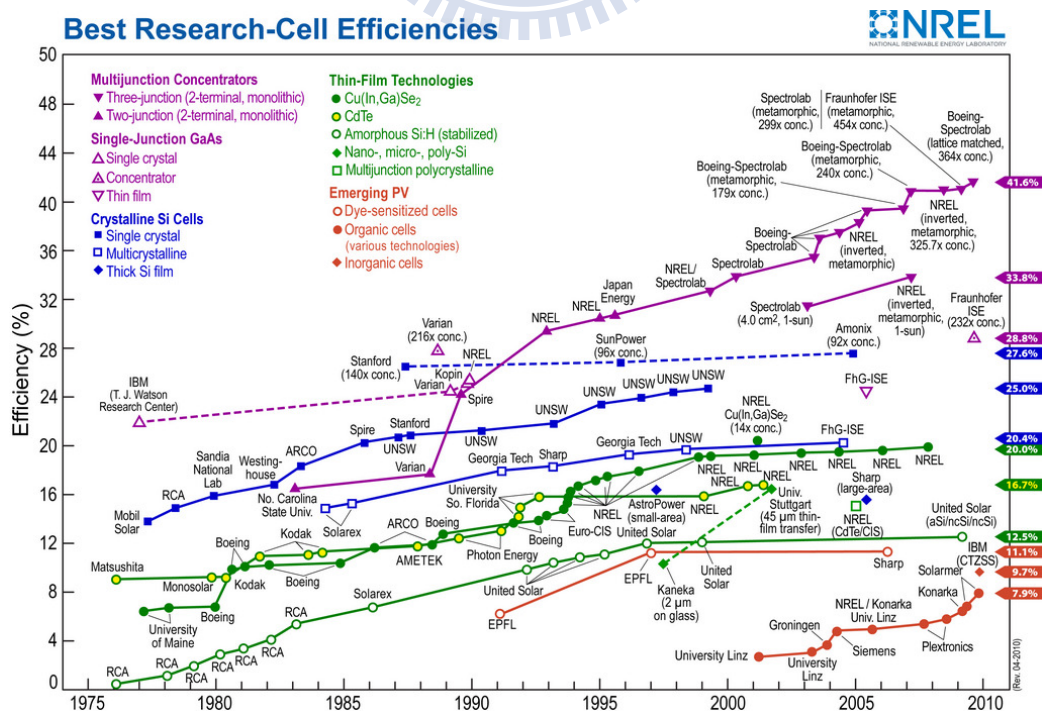
Fig. 1-2   The progress of the best research-cell conversion efficiencies

1.2.2 Thin Film Solar Cell Technology

There are several categories in thin film solar cell technology including silicon thin film, CdTe, CIS / CIGS, and Organic / polymer solar cell. The following are some introduction and characteristics about these thin film solar cells:

Cadmium Telluride (CdTe): With an optimal band-gap of 1.44 eV, CdTe is an efficient light-absorbing material for thin film cells. The cell thickness only need to be around 1 μm, significantly reducing the material costs. Efficiencies close to 10 % have been achieved in commercial modules by Solar Cells Inc. However, the toxicity of CdTe-based solar cell on health and the environment is still a concern.

Copper Indium (Gallium) Selenide (CIS / CIGS): These semiconductors are attractive for their high optical absorption coefficient and versatile optical and electrical characteristics can be manipulated to fit the needs for device. The best efficiency of CIGS solar cell has achieved 19.9 % in 2008 [1]. By using optical concentrator or multi-junction tandem solar cell, higher efficiencies (>30 %) can be obtained. But the manufacturing costs of CIGS solar cells are high when compared to hydrogenated amorphous silicon (a-Si:H) solar cells.

Organic / polymer solar cell: These devices don't rely on built-in electric field like inorganic solar cells. The active layer consists of two materials, one acts as an electron donor and the other as an acceptor. The efficiencies of organic / polymer solar cell has quickly improved in recent years and the best one has achieved 6.77 % [2]. But the stability and excitation diffusion length should be enhanced in the future.

Silicon thin film: In Earth's crust, silicon is the second most abundant element after oxygen, making up 25.7 % of the crust by mass. That is the reason for hydrogenated s-Si p-i-n solar cells is the most studied alternative energy method. Furthermore, the multi-junction technology can be also applied combining a-Si:H with μc-Si:H solar cells. Triple stack a-Si:H / μc-Si:H / μc-Si:H achieved module efficiency of up to 12 % with much less photo-degradation [3]. Our group also focuses on this silicon thin film solar cell field.

1.2.3 Silicon Thin Film Solar Cell Technology

Silicon thin film solar cell consists of a-Si:H or microcrystalline silicon (μc-Si:H) materials. Compared to crystalline silicon (c-Si) solar cell including single crystalline or multi-crystalline silicon, the light absorption coefficient of silicon thin film solar cell is much higher, as shown in Fig. 1-3. Thus, the thickness (~1 μm) and silicon material consumption can be effectively reduced, which can lower the solar cell cost.
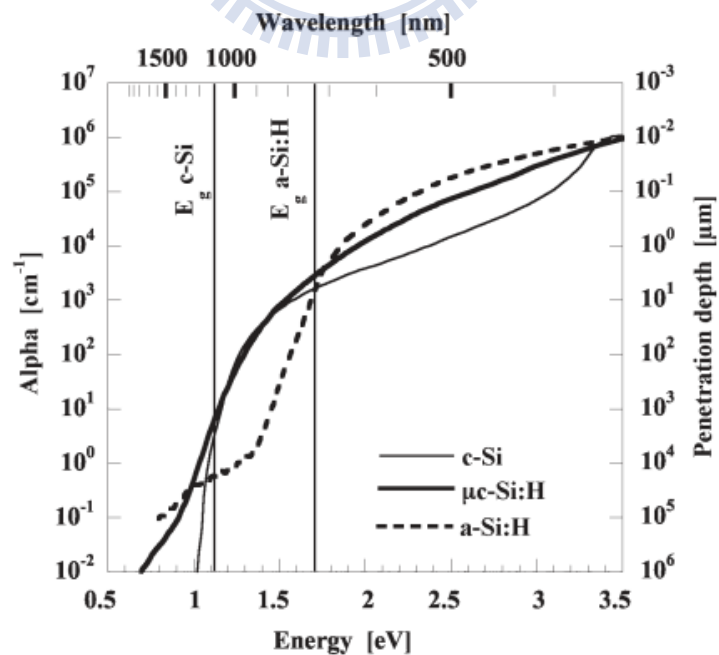
Fig. 1-3   Absorption coefficient α vs. energy for a-Si:H, μc-Si:H and c-Si [4]

Both a-Si:H and μc-Si:H solar cells have two stack types: p-i-n and n-i-p.   We focus on p-i-n structure in this thesis, as shown in Fig. 1-4. In this configuration, light enters from the p-layer side. The internal electric field is built up by the Fermi level difference between p- and n-layer. For light impingement, electron-hole pairs are created in the intrinsic μc-Si:H layer (i-layer), which is the "charge separation" process. Then, "charge transportation" happens because of the internal electric field. During the transportation process, "charge recombination" occurs due to defects in the films. "Separation, transportation, and recombination" are the working mechanism for solar cell to convert light to electricity.
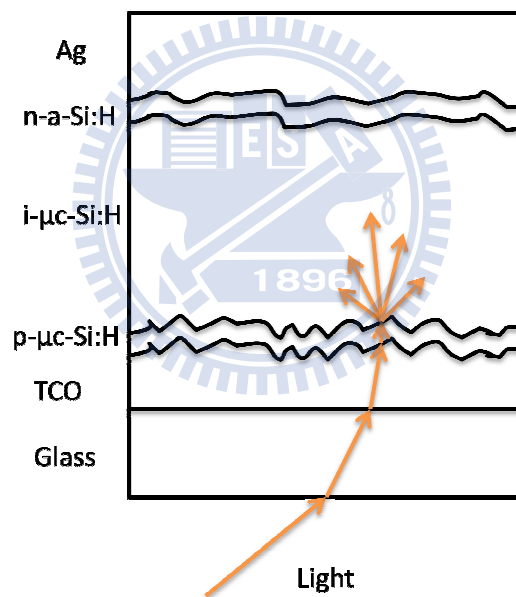
Fig. 1-4   Schematic diagram of a single junction μc-Si:H p-i-n solar cell structure

Due to the direct band-gap property, a-Si:H solar cell has good optical absorption ability in visible spectrum. The preparing method of a-Si:H is mature and low cost. The thin film can be deposited on glass, metal or plastic substrate. But the serious light degradation is one big problem should be improved.

The structure of μc-Si:H is between a-Si:H and c-Si, there are some crystalline parts incorporate into amorphous network. Because of such structure, μc-Si:H also possesses the advantages of a-Si:H including good optical absorption ability and low cost. Furthermore, the light degradation of μc-Si:H is much less than that of a-Si:H.

There is a fascinating structure with the combination of both a-Si:H and μc-Si:H material. It is because the bandgap difference between a-Si:H (~1.8 eV) and μc-Si:H (~1.12 eV), their maxima light absorption spectrum peak are different as well. For a-Si:H, the peak is toward short wavelength; for μc-Si:H, the peak is toward long wavelength. Thus, combination of these two type materials could achieve a substantial increase of conversion efficiency due to broader light spectrum absorption.

1.3 Motivation

In order to enhance the conversion efficiency as well as to upgrade the performance per cost of silicon solar cell, this series of experiments investigates the characteristics of thin film material. We attempt to understand which material properties could improve the conversion efficiency and endeavor to manipulate these material properties by controlling appropriate process parameters. Consequently, a series of experiment on silicon thin film solar cell have been done in this thesis.

Chapter 2   LITURATURE REVIEW

2.1 Hydrogenated Amorphous Silicon

Two kinds of silicon base material is used in this study: μc-Si:H and a-Si:H. Fig. 2-1a shows the structure of c-Si schematically. Silicon is a four-fold coordinated atom that is normally tetrahedral bonded to four neighboring silicon atoms. The unit cell and its duplicates next to each other, the regular atomic arrangement is described as a structure with long range order. Fig. 2-1b illustrates that a-Si:H does not have well-ordered structure. Though a-Si:H lacks long range order, it has short ranger order same as c-Si. Due to the short range order the concept of the energy state bands, represented by the conduction and valence bands can be adapted to a-Si:H. Unlike c-Si epitaxial growth should be taken at high temperature around several hundred Celsius and grows on silicon wafer, the a-Si:H can be deposited at low temperature and on flexible or glass substrates. With this advantage a-Si:H is suitable option for roll to roll mass production. However, as shown in Figure 2-2b the deviation in bond angles and bond lengths between a-Si:H bonds result in weak and strained bonds which are easier to be broken if they absorb enough energy, for example in the form of heat or radiation. The process is a leading cause of defect formation in the atomic network. Those defects in a-Si:H random network are noted as coordination defects [5]. That the reason why a-Si:H is a defect-abundant material. The defect density of pure a-Si:H is about 10^{21} cm^{-3}. Such material with so high defect density cannot be applied to electronic devices. a-Si:H can be deposited by plasma-enhanced chemical vapor deposition (PECVD) from silane (SiH$_4$). The hydrogen from SiH$_4$ can be incorporated into a-Si:H network and form stronger silicon-hydrogen bonds. Therefore, in a-Si:H structure, the defect density decreases dramatically to 10^{15}-10^{16}

cm^{-3} due to dangling bond passivated by hydrogen radical. This material can be a candidate for electronic application.
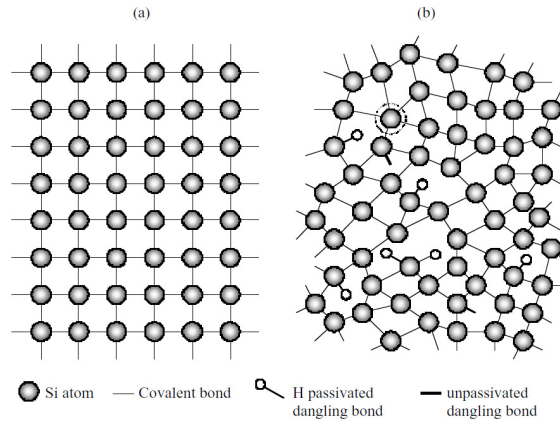
Fig. 2-1   Schematics representation of the atomic structure of (a) c-Si, (b) a-Si:H [6]

Since the first report of depositing high quality a-Si:H with hydrogen dilution [7] , the hydrogen dilution method is widely used to improve the quality of a-Si:H. The mechanisms in hydrogen dilution SiH$_4$ plasma are concluded by S. Sriraman, et al [8]:

1.   Hydrogen provides improved surface coverage that results in the impinging molecules diffusing further to find more favorable sites [9-10]

2.   Hydrogen etches away the disordered regions, leaving behind the ordered structure [11-13]

3.   Hydrogen atoms can be inserted into strained Si-Si bonds in the sub-surface region through the formation of a SiH$_n$ complex—structural relaxation (more ordered phase) [14-17]

Using hydrogen dilution can improve open-circuit-voltage (V$_{oc}$) of solar cells due to the increase of hydrogen concentration in a-Si:H. The etching mechanism can remove the weak structure in a-Si:H bonding network and leave the solid structure, effectively enhancing the quality of a-Si:H film.

2.2 Doping of Hydrogenated Amorphous Silicon

Doping by furnace is widely used for the doping of c-Si. Silicon wafers are put into the furnace and the dopants are introduced in the furnace at the same time. The dopants evaporate at such high temperature (900 ℃~950 ℃) and diffuse into silicon wafers. From W. Spear's report [18], the conductivity of n- and p-type a-Si:H as a function fraction of doping gases in the gas mixture with SiH_4 was shown in Fig. 2-2.
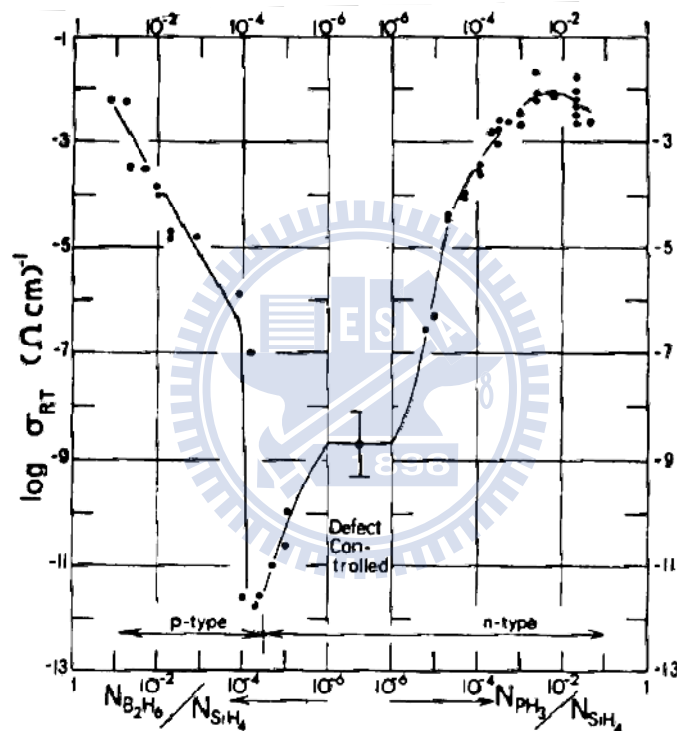
Fig. 2-2   Room temperature conductivity, σ_{RT}, of n and p-type a-Si:H plotted as a function fraction of doping gases in the gas mixture with SiH_4 [18]

Unlike c-Si, the chemical reaction in PECVD is a gas phase reaction, the doping of a-Si:H can be achieved by the introduction of doping source gases like B_2H_6、TMB、 PH_3 as the deposition of amorphous silicon in PECVD system.

2.3 P-i-n structure of silicon based solar cell

There are three main physic mechanisms responsible for the collection of photo-generated carriers in p-n diode photovoltaic:

1. The drift current of holes and electrons in depletion region.
2. The diffusion current of minority carriers in n-type neutral region
3. The diffusion current of minority carriers in p-type neutral region

In typical mono-crystalline and poly-crystalline silicon p-n diode photovoltaic, the contribution of photo-generated carriers in depletion region is trivial due to the width of this region is too thin compared to the diffusion length of minority carriers. The main current of mono-crystalline and poly-crystalline solar cells is diffusion current in neutral region. The absorption coefficient of a-Si:H is about two orders higher than c-Si, the material needed in a-Si:H thin film solar cells is 1 % of c-Si solar cells needed. However, a-Si:H is a defective material. The diffusion lengths are so short in doped a-Si:H, the undoped region is needed to extend the thickness which photons can be absorbed effectively. The thin p-layer and n-layer form the built-in field which drives charges separation. In the p-i-n structure photocarriers are collected primarily by drift rather than by diffusion. Fig. 2-3 shows the band diagrams and sketches of p-n and p-i-n structures.
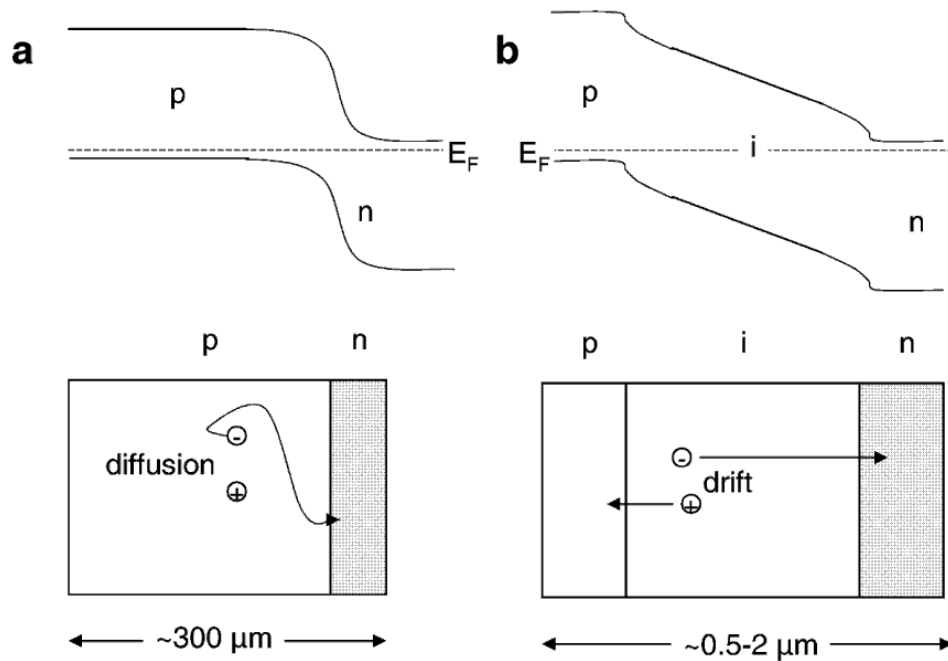
Fig. 2-3   Band diagram and sketch of a (a) p-n and (b) p-i-n cell [19]

2.4 Plasma-Enhanced Chemical Vapor Deposition

Many growth methods have been proposed to fabricate a-Si:H and μc-Si:H, e.g. hot-wire CVD, photo CVD, PECVD. Among these growth methods, PECVD system is widely used because its low substrate temperature during deposition (less than 300 ℃), good uniformity ,and large scale productions.

PECVD is a deposition method where reactive species are produced by an electrical discharge leading to plasma. The gas-phase reactions in glow discharges reduce the substrate temperature required for film deposition compared to thermal CVD, so more compatible substrates can be used in this deposition process (like glass, stainless steel, or plastic substrate). In order to yield a high quality silicon thin film, electron impact dissociation of source gas, gas-phase reaction, radical diffusion and surface reaction have to be considered [20]. In this study, SiH_4 and H_2 are the source gas which is dissociated into reactive neutral and ions species by electron impact excitation in plasma. And these reactive neutral and ions species have the secondary

11

reactions with parent SiH_4 and H_2 molecules while they diffuse to the substrate [21], as shown in Table. 2-1. All the possible reactive neutral and ions species in plasma is given in reference [22]. Then, their reactive products interact with the surface of growing film, such as radical diffusion, chemical bonding, and hydrogen sticking to the growing film or re-emitted from the surface to gas phase.

Table. 2-1　The function of primary reactions and secondary reactions [22]

Primary reactions	Secondary reactions
$e + SiH4 \rightarrow SiH_2 + H_2 + e$	$SiH_4 + H \rightarrow SiH_3 + H_2$
$SiH_3 + H + e$	$SiH_4 + SiH_2 \rightarrow Si_2H_6$
$SiH + H_2 + H + e$	$SiH_3 + SiH_4 \rightarrow SiH_4 + SiH_3$
$SiH_2 + H_2 + 2e$	$SiH_4 + Si_2H_6 \rightarrow Si_nH_m$
$SiH_3^+ + H + 2e$	
$SiH_3^- + H$	

Fig. 2-4 shows two typical configurations of a-Si:H solar cells with p-i-n structure. Form Fig. 2-4a substrate of the superstrate structure is usually the SnO_2 or ZnO coated glass. The textured surface of TCO coated glass can improve the ability of light-trapping to the absorption of solar cells. From Fig. 2-4b, the substrate of substrate structure can be flexible materials like stainless steel or plastic.

Both configurations are usually illuminated through a TCO / p-layer interface. The short-wavelength light is mainly absorbed at the surface of solar cells, due to the short depth of penetration. The mobility of hole is much smaller than electron. For more efficient collection of photo-generated carriers and avoiding the recombination of holes, plane of incidence of light is usually p-layer which is also called as window layer in solar cells.
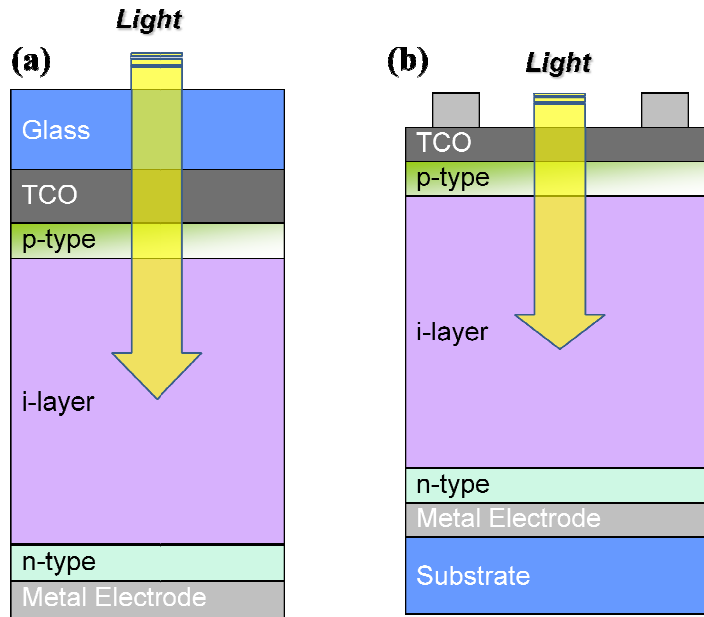
Fig. 2-4 (a) The superstrate cell configuration and (b) the substrate cell configuration

2.5 Hydrogenated Microcrystalline Silicon

μc-Si:H is a material which consists of crystalline grains, amorphous phase and voids, and the grain size usually in μm range or smaller. The actual structure of the material depends strongly on the deposition conditions and has a strong impact on the device performance. μc-Si:H is a non-homogenous material, even though with the same deposition parameters, different deposition times make large difference in crystallinity value and other relating characteristics. A structural model of μc-Si:H material is shown in Fig. 2-5.

Fig. 1-3 shows the absorption spectra of a-Si:H, μc-Si:H and c-Si. The absorption coefficient of a-Si:H for photon energies above 1.8 eV is much higher than in crystalline and μc-Si:H. Due to the lower optical absorption coefficient, the incident light is absorbed almost completely in film thicknesses below 1 μm. But a lower mobility gap of μc-Si:H lead to a benefit of light absorption in the near infrared

13

region.
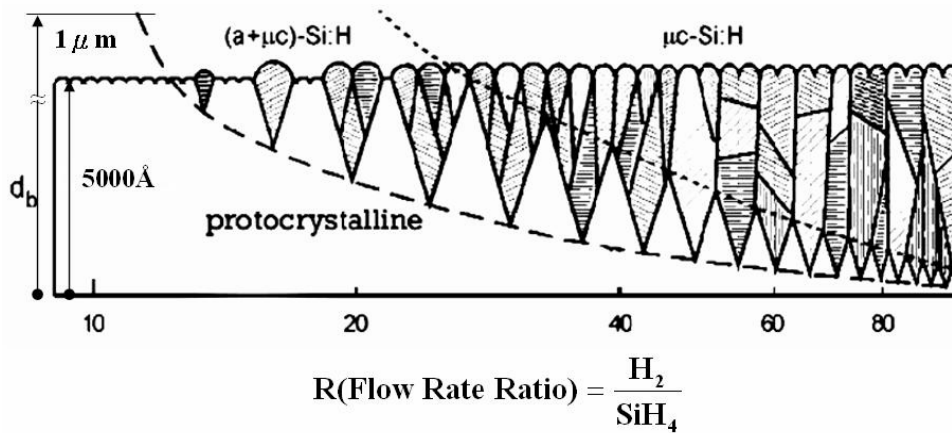
Fig. 2-5   Influence of hydrogen dilution ratio and thickness on crystallinity [23]

There are three models have been proposed : surface diffusion model [24], etching model [13] and chemical-annealing model [25]

2.5.1 Surface Diffusion Model

The crystalline volume fraction of deposited films strongly depends on the surface diffusivity of SiH_x which is improved when the SiH_4 concentration is reduced or the substrate temperature increased. This is due to the hydrogen surface coverage improvement prolong the SiH_x surface diffusion length to permit SiH_x to attach at favorable sites to create a flat film surface. This has been confirmed by the abrupt fall of the film crystallinity for substrate temperature higher than $400^{\circ}C$ [26], caused by the desorption of hydrogen adsorbed on the surface at such high temperatures [27]. Moreover, some of the hydrogen atoms coming from the plasma recombine with surface bonded-hydrogen heating locally the surface, which enhances the surface diffusion of SiH_x as sketched in Fig. 2-6. The role of the surface diffusion in flattening the film surface is of particular importance for the nucleation of crystallites as shown

14

by in-situ spectroscopic ellipsometry studies. They have shown that silicon crystallite nucleation needs a smooth surface and occurs only after a reduction of the initial surface roughness. This shows that to promote the crystallinity of the deposited silicon film, a sufficiently high atomic hydrogen flux towards the growing film surface has to be delivered with respect to the silicon radicals flux. However, the role of the SiH_x surface diffusion in µc-Si:H growth may not be dominant for depositions performed at high rates, because of the shorter time allowed for SiH_x radicals to find adequate sites to attach.
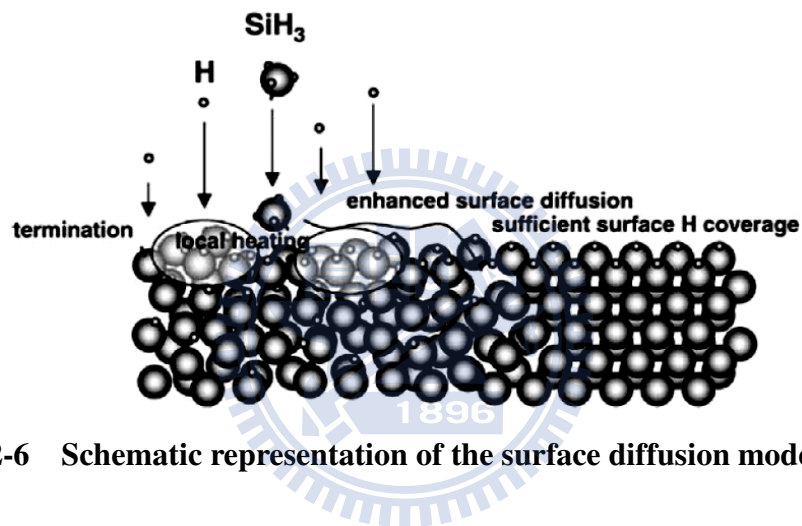
Fig. 2-6   Schematic representation of the surface diffusion model [28]

2.5.2 Etching Model

The diffusion model was able to explain µc-Si:H deposition for substrate temperatures lower than 400◦C, but µc-Si:H deposition at higher temperatures [29] shows that this model is not sufficient. A combination of the surface diffusion model and selective etching model may explain the deposition of µc-Si:H. This selective etching model is based on the experimental observation of silicon etching by hydrogen [30] by the reverse chemical reaction leading to silicon deposition from SiH_4 discharge [13]

$$SiH_4 \longleftrightarrow Si_{film} + 4H \qquad \text{(Eq. 2-1)}$$

This model is called selective because of the different etching rate of a-Si:H and

μc-Si:H [30]. Indeed, the high lattice defect density in the amorphous structure facilitates the atomic hydrogen to etch the silicon atoms which are weakly bonded to their neighbors, whereas the well-arranged silicon atoms of the crystallites resist better to hydrogen etching [28]. The selective etching model sketched in Fig. 2-7 is based on the hypothesis that both a-Si:H and μc-Si:H are deposited and etched simultaneously, but with an etching rate much higher for the amorphous phase, hence increasing the crystalline volume fraction of the growing film. This model has to be combined with the surface diffusion model in order to explain the nucleation of the crystallites to initiate the μc-Si:H growth from the initial a-Si:H incubation layer. As for the surface diffusion model, the crucial physical consideration is the atomic hydrogen flux towards the film surface with regard to the silicon radical flux, in order to etch efficiently the amorphous phase to promote the film crystallinity.
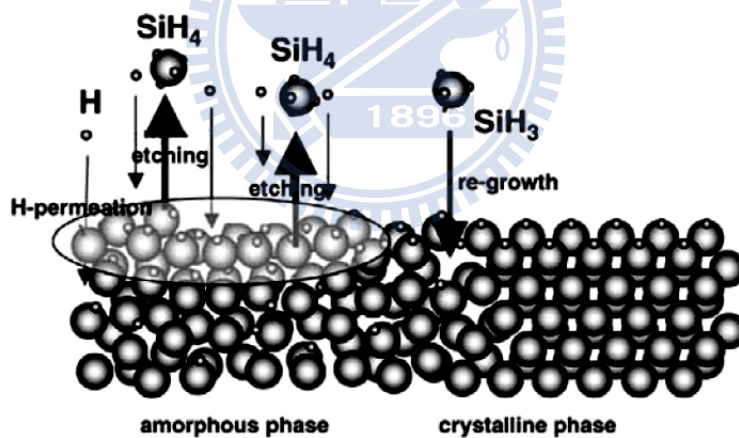
Fig. 2-7   Schematic representation of the selective etching model [28]

2.5.3 Chemical Annealing Model

The chemical annealing model has been constructed in order to explain the crystallization of a-Si:H when exposed to a pure H_2 plasma [25]. Indeed, μc-Si:H can be produced by using a layer-by-layer technique by alternatively depositing a thin a-Si:H layer and expose it to a pure H_2 discharge which crystallizes the thin layer.

Neither the etching model, nor the surface diffusion model, can explain this phenomenon. This third model is based on the chemical reaction of atomic hydrogen coming from the plasma with hydrogen bonded to silicon at the film surface or sub-surface as depicted in Fig. 2-8 . The reaction creates a silicon dangling bond and a hydrogen molecule. This reaction is exothermic, and the resulting structure thermal vibration promotes surface and bulk structural rearrangement leading to the energetically more favorable μc-Si:H . The Si dangling bond created is then transformed into a more stable and rigid Si-Si bond or, if placed at the film surface, re-hydrogenated by atomic hydrogen from the plasma. In the selective etching model, the H atoms attach to silicon and re-hydrogenate the bulk silicon until SiH_4 desorption. But in the chemical annealing model, the H atoms recombine with surface or sub-surface hydrogen.

Consequently, the atomic hydrogen flow rate towards the surface has to be large compared to the silicon radical flux to promote the growth of μc-Si:H. This is to increase the surface diffusivity by a fully H-covered surface, to remove undesirable a-Si:H by selective etching by H atoms, or to generate vibrational energy by hydrogen surface or sub-surface recombination, according to the surface diffusion, the selective etching or the chemical annealing models, respectively.
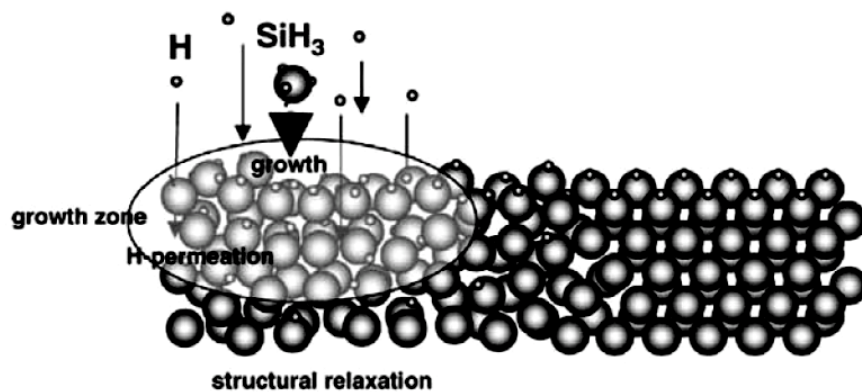
Fig. 2-8   Schematic representation of the chemical annealing model [28]

2.6 Stabler-Wronski Effect

Electrical properties of a-Si:H would be changed under long time light exposure. This phenomenon is well-known as Staebler-Wronski Effect discovered by D.L. Staebler and C.R. Wronski in 1977 [31]. Weak bonds in a-Si:H like dihydride、 trihydride bonds and cluster of Si-H may be broken and result in the formation of dangling bonds by long time illumination of light. When the defect density of dangling bonds increases, the lifetime of photo-generated carriers reduces. Due to the strong recombination loss through the localized states formed by the dangling bonds in a-Si:H network, the conversion efficiency degraded severely in a-Si:H based solar cells [32-33].

However, an essential feature of light-induced effects on a-Si:H film and solar cell can be reversible by annealing above 150℃. The performance of stabilized a-Si:H solar cells is 70 ％ to 85 ％ of their initial efficiency depends on the quality of a-Si:H film. This light-induced degradation is the major disadvantage of a-Si:H as a photovoltaic material.

2.7 a-Si:H / a-Si:H Tandem Solar Cell

An important issue of a-Si:H single junction solar cell is the light-induced degradation in conversion efficiency. The stability have been improved by stacking a-Si:H multi-junction cell, because each i-layer thickness of top and bottom cell is thinner than in a a-Si:H single junction cell [34]. Wieder et al. [35] reported an initial efficiency of 9.2 ％ with a relative decrease of 8 ％ in the efficiency after 900 hours light soaking. This improvement is because the carrier extraction is more effective in thinner thickness of i-layer. To obtain the best cell efficiency, current matching between top and bottom cell should be considered. If the current matching is properly

made, the initial efficiency of a-Si:H / a-Si:H tandem solar cell is approximately equal to the single junction cell with the same i-layer thickness.

The junction between the top and bottom cell usually called tunneling recombination junction (TRJ). The photo-generated electrons from top cell and the photo-generated holes from bottom cell flow in this junction. These carriers should be recombined because of the accumulation of carriers which would weaken the electric field in the top and bottom cell. Therefore, the recombination should be strong in TRJ. Moreover, the TRJ has to be ohmic contact between top and bottom cell, and low optical absorption is also required. There were many kinds of TRJ is applied in a-Si:H / a-Si:H tandem solar cell like :

•   n-μc-Si:H / p-a-Si:H [36]:

    The n-μc-Si:H strongly reduced n-p contact resistance

•   n-μc-Si:H / μc -a-Si:H [37]:

    Improving the recombination at the junction

•   n-a-Si:H / n-μc-Si:H / p-μc-Si:H [38]:

    To protect the first deposited subcell from the damage

•   oxide / n-μc-Si:H / oxide / p-μc -Si:H [38]:

    Improving nucleation and creating a defective interface layer to enhance

    recombination

•   n-μc-Si:H / i-μc-Si:H / p-μc-Si:H [39] :

    More reproducible than oxided interface

2.8 Microcrystalline Silicon Single Solar Cell

SiH_4 depletion and high pressure have been observed to improve crystallinity and film quality at high deposition rate [40], and this condition is so-called high pressure depletion region. In high pressure region .The SiH_4 react with atomic hydrogen as

19

follows:

$$SiH_4 + H \rightarrow SiH_3 + H_2$$
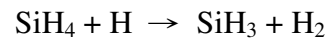
This might cause the deterioration of crystallinity. At high power condition, the high
dissociation rate leads to SiH_4 depletion and then the annihilation reaction is
suppressed. There are many groups used this region to deposit μc-Si:H solar cells, and
high cell efficiency [28, 41-45] and high deposition rate [45] is achieved.

Chapter 3   EXPERIMENT DETAILS

In this study, μc-Si:H thin film is deposited on Corning Eagle 2000 and All Solar cells are deposited on 3.9 mm thick glass with transparent conductive oxide (SnO_2:F) on it. These two kinds of substrates are cleaned by KG cleaner before the deposition. The thickness of μc-Si:H thin film is measured by α-step.

The sequence of a-Si:H / a-Si:H tandem solar cell deposition is p-doped layer / intrinsic layer / n-doped layer / p-doped layer / intrinsic layer / n-doped layer / back TCO / A_g. The back TCO (GZO) is prepared by sputtering, and the silver contact is prepared by thermal evaporation.

3.1 PECVD System

Both a-Si:H and μc-Si:H were prepared by radio-frequency (27.12 MHz) PECVD system. In Fig. 3-1, the substrate is transferred on the heater. A showerhead electrode is used in this system, and source gas is fed in at the upper electrode. This electrode design improves the homogenous gas composition and so does the uniformity of silicon thin film [46-47]. The area of showerhead electrode is 26x26 cm^2 and the volume of reaction chamber is 33.6 liter. All the samples were deposited until the background pressure reach to $5x10^{-4}$ Pa. Doping layers were prepared by using CH_4, B_2H_6 or PH_3 with SiH_4 and H_2 dilution. In solar cell fabrication process, the reaction chamber is cleaned by Ar and NF_3 plasma between intrinsic layer and doping layer to avoid cross contamination.
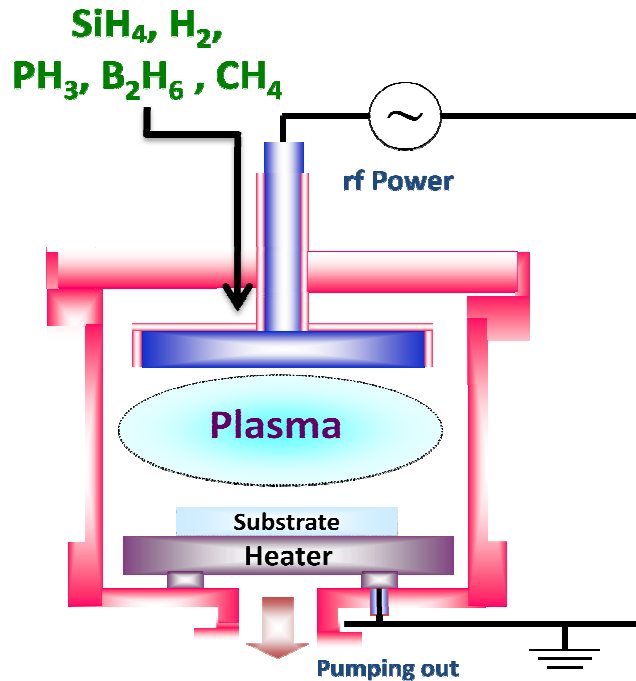
Fig. 3-1   Schematic view of PECVD system

3.2 AM 1.5 Light Source

The conversion efficiency of solar cells has straight connection to the intensity and spectrum of incident solar radiation. However, as the sunlight travels though the atmosphere, chemicals react with the sunlight and absorb certain wavelengths. For the well-known example is the stripping of ultraviolet light by ozone in the upper atmosphere, which drastically reduces the amount of short wavelength light, reaching the Earth's surface. Additionally, water vapor, nitrogen, oxygen and carbon dioxide in atmosphere results in a wide variety of absorption bands at many wavelengths

Generally, we use the air mass (AM) conception to define the absorption, scattering and reflection in the atmosphere and the location and angle of solar cells

$$\text{Air mass} = 1 / \cos \theta \qquad \qquad \text{(Eq. 3-1)}$$

θ means the included angle between the incident angle of sunlight and ground. As shown in Fig. 3-2, the spectrum outside the atmosphere, the 5,800 K black body, is referred to as "AM0", meaning "zero atmospheres". Cells used for space power

22

applications, like those on communications satellites are generally characterized using AM0.

The spectrum after traveling through the atmosphere to sea level with the sun directly overhead is referred to as "AM1". This means "one atmosphere". Conveniently, silicon solar cells are not very sensitive to the portions of the spectrum lost in the atmosphere. Since solar cell development is concentrated in the United States, Europe and Japan, an AM number representing the spectrum at mid-latitudes is much more common. "AM1.5", 1.5 atmosphere thicknesses, corresponds to a solar zenith angle of 48.2°, and is almost universally used to characterize solar panels.
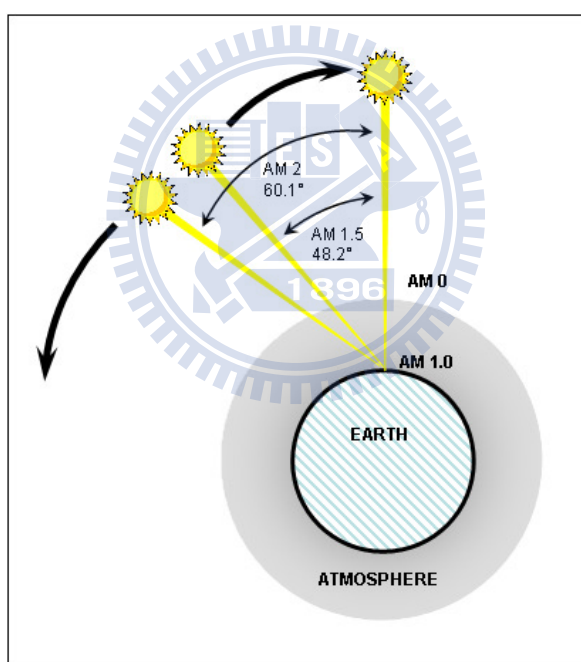
Fig. 3-2　Schematics of air mass

3.3 Material Analysis Equipment

3.3.1　Raman spectroscopy

Raman spectroscopy is the fastest and the easiest experimental technique for crystallinity measurement. The Raman effect, first reported by Raman and Krishna in

1928 [48], has been used to investigate the structure property of μc-Si:H. The theory of this method is given in literature [49]. The Raman apparatus used in this study was a HORIBA, Labram HR raman microscope with an He-Ne laser source (633 nm).
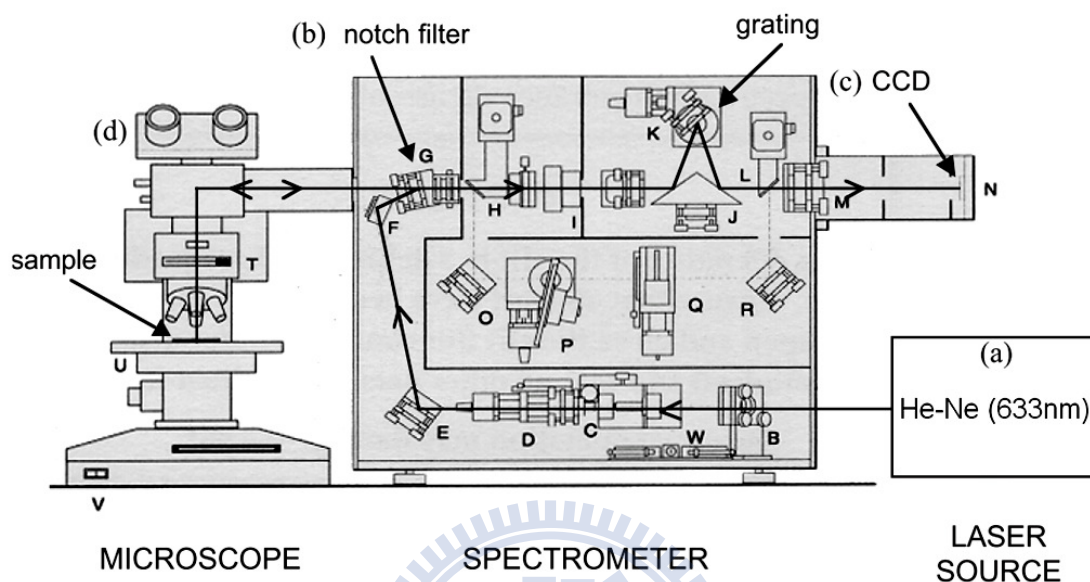
Fig. 3-3   Micro-Raman spectrometer composed of an He-Ne laser source, a microscope, a notch filter, a grating and a CCD camera [50]

Fig. 3-4 shows Raman spectrum as a sample. In Raman spectroscopy, a-Si:H result in the occurrence of a board peak at about 480 cm^{-1}. The integrated intensity of this peak I_a is proportional to the amorphous volume fraction in the volume. The signal of μc-Si:H is a narrow peak at 520 cm^{-1}, which is the position of the transverse optic mode in monocrystalline silicon. Another narrow peak occurs at about 510cm^{-1} is because of the defective part of the crystalline phase (crystallites smaller than 10 nm [51], or to a silicon wurtzite phase [52] that result from twinning [53]). So the crystalline volume fraction can be considered proportional to the peaks at 510 cm^{-1} and 520 cm^{-1} and the equation below can be obtained by the deconvolution and integration of Raman lines. X_c is a useful factor to quantify the crystallinity of μc-Si:H thin films.

$$\mathbf{X_c} \text{ (crystallinity)} = \frac{I_c}{I_a + I_c} = \frac{I_{510} + I_{520}}{I_{480} + I_{510} + I_{520}} \qquad \textbf{(Eq. 3-2)}$$
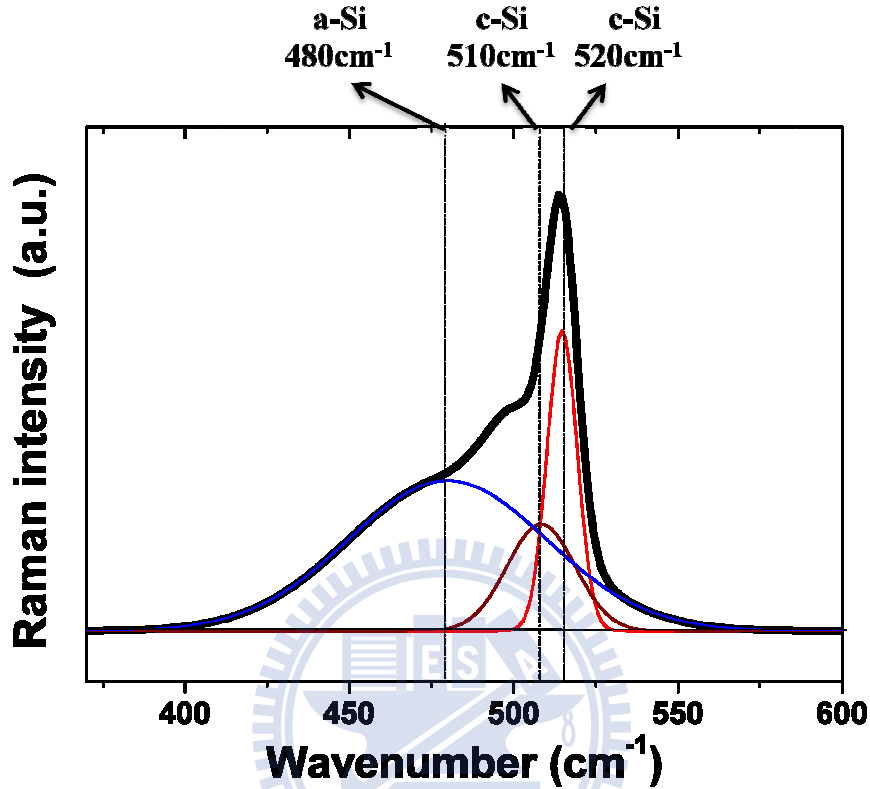
Fig. 3-4   Raman spectrum of μc-Si:H

3.3.2 XRD

X-Ray diffraction is a method to gain information about crystal structure, orientations and crystal defects [54] based on Bragg's equation. XRD analysis was carried out by Bede, D1 diffractometer with 2θ scan (Bragg-Brentano geometry) with an angle step of 0.1° and a signal collection time of 1 s. CuK$_\alpha$–radiation characterized by a wavelength of λ=1.542 Å (~8 KeV) was initiated by a voltage of 40 KV and a current of 40 mA.

3.3.3 Photo (σ_{ph}) and dark conductivity (σ_d)

Photo (σ_{ph}) and dark conductivity (σ_d) of intrinsic films were investigated by coplanar conductivity measurements at room temperature, and σ_{ph} is measured under AM1.5 illumination. This is one way to obtain the information about material characteristic of μc-Si:H and a-Si:H. Besides, the photosensitive (σ_{ph} / σ_d) is an useful parameter to see the transition region of a-Si:H to μc-Si:H or the property of a-Si:H [20]. The σ_d of a-Si:H used in devices should be lower than 10^{-10} Scm^{-1}, and the σ_{ph} should be higher than 10^{-5} Scm^{-1}. Therefore, the photosensitive for a good quality a-Si:H thin film should be higher than 10^5 [20]. For μc-Si:H, the σ_d , σ_{ph} and photosensitivity usually around 10^{-7} , 10^{-5} and 10^2 respectively [55-56].

In order to investigate the conductivity of the μc-Si:H thin film , metal contacts were deposited onto the silicon thin film by thermal evaporation. Conductivity is calculated by Eq. 3-3, where V and I are the bias voltage and measured current, respectively. The other relative parameters in equation Eq. 3-3 are shown in Fig. 3-5.

$$\sigma = \left(\frac{I}{V}\right) \left(\frac{L}{W}\right) \left(\frac{1}{t}\right) \qquad \textbf{(Eq. 3-3)}$$
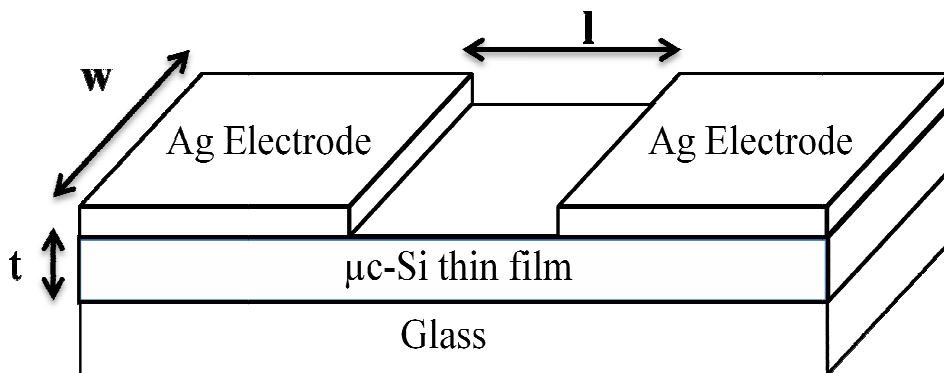
Fig. 3-5   Schematics of the conductivity measurement

3.4 Solar Cell Characteristic

3.4.1 Current-Voltage Characteristics

The measurement of I-V characteristics is the primary method to evaluate solar cells. It is measured under AM 1.5 light source.

- The efficiency (η) is defined as the ratio of the maximum power generated by the device and the radiation power incident in the area of cell.

- The short-circuit current density (J_{sc}) is the maximum current density generated by the device under light illumination.

- The open-circuit voltage (V_{oc}) is the maximum voltage generated by the device under light illumination.

- The fill factor (F.F.) is defined as a ratio of maximum power generated by the cell and the ideal power generated which is equal to $J_{sc} \times V_{oc}$. This factor relate to the shunt resistance, series resistance and material quality in the device.

3.4.2 Quantum Efficiency

Spectral response provides the information about the working principle of solar cell. The Quantum efficiency is defined as

$$Q.E. = \frac{J_{ph}(\lambda)}{e \times \varphi(\lambda)} \qquad \text{(Eq. 3-4)}$$

where, J_{ph} is the photo-generated current density per wavelength interval e is the elementary charge, and ϕ is the number of photon per time, area, wavelength interval. Therefore the quantum efficiency describes the probability that an incident photon generates a charge carrier pair which contributes to the photo current.

Chapter 4   RESULTS AND DISCUSSIONS

4.1 Effect of Methane to Silane Flow Rate on film Property of p-type Amorphous Silicon

Fig. 4-1 illustrates the deposition rate of p-type amorphous silicon carbide (a-SiC:H) as a function of CH_4 to SiH_4 flow rate ratio. Besides, the hydrogen to SiH_4 ratio was 2.5, the deposition pressure was controlled at 80 Pa. From Fig. 4-1, the deposition rate decreased with the increase of CH_4 to SiH_4 flow rate ratio. The main reason for this result can be attributed to the main source gas of p-type a-SiC:H deposition. The reduced concentration of SiH_4 in plasma reasonably lowered the deposition rate.
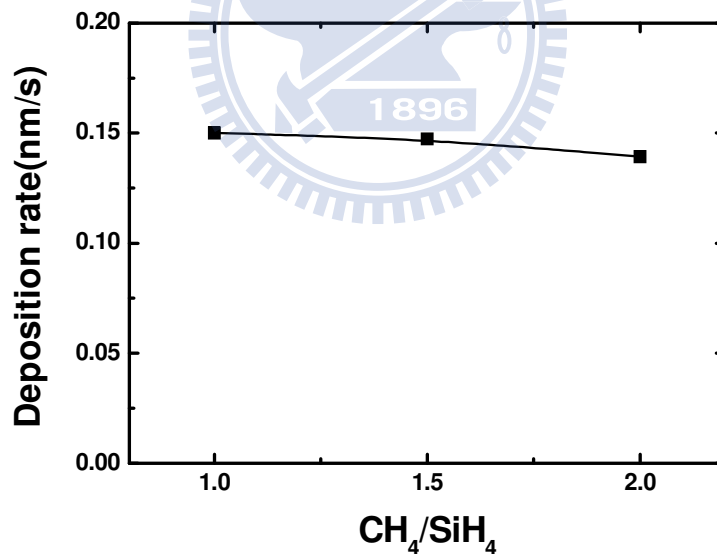
Fig. 4-1   The deposition rate of p-type a-SiC:H as a function of CH_4 to SiH_4 flow rate ratio
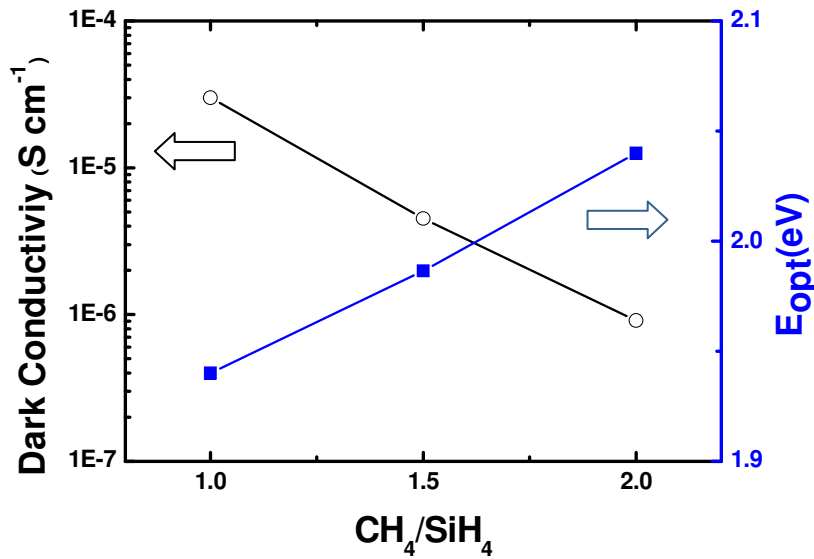
Fig. 4-2   The optical bandgap and dark conductivity of p-type a-SiC:H as a function of CH$_4$ to SiH$_4$ flow rate ratio

The optical bandgap and σ_d of p-type a-SiC:H as a function of CH$_4$ to SiH$_4$ flow rate ratio can be observed Fig. 4-2. The optical bandgap apparently enlarged and σ_d drastically decreased with the increasing ratio of CH$_4$ to SiH$_4$.

More carbon was incorporated into a-Si:H film with increasing the concentration of CH$_4$ in source gases. The binding energy of Si-C is larger than Si-Si, consequently, the introduction of CH$_4$ when depositing p-layer can enlarge the optical bandgap. However, the conductivity decreased as increasing the content of carbon in a-Si:H network. P-type a-SiC:H was served as a window layer and emitter layer in our cells. The values of electric conductivity and optical bandgap of p-layer should be a trade-off issue. The bandgap and σ_d should be larger than 2.0 eV and 1×10^{-5} Scm^{-1}, respectively of optimal p-layer [20].

4.2 Characteristic of Amorphous Silicon n-type Layer

The purpose of doping is to change electrical conductivity and its magnitude by

adding a controlled amount of special impurity atoms. The principal doping elements used in a-Si:H are the same as in c-Si : boron for p-type and PH_3 for n-type material. We achieved a change in conductivity of a-Si:H the silicon source gas, SiH_4, with PH_3 during deposition using the glow discharge method [57]. The n-type a-Si:H is mixing SiH_4 and PH_3 to change conductivity. From Fig. 4-3, the σ_d as function of SiH_4 and B_2H_6 flow rate ratio. As shown in Fig. 4-4.

As shown in Fig. 4-3, the bandgap as function of PH_3 to SiH_4 ratio. The band gap and σ_d didn't change too much. From Fig. 4-3, the trivial differences in σ_d of n-type a-Si:H can be attributed to the experimental deviation.
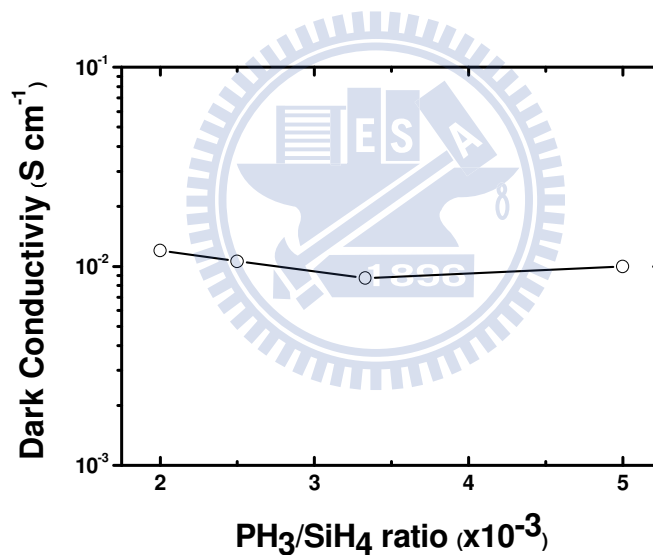
Fig. 4-3   Dark conductivity as function of PH_3 to SiH_4 ratio
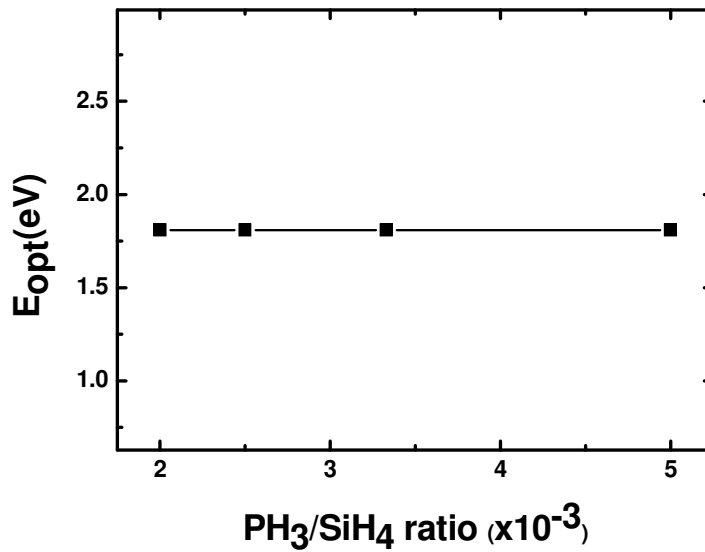
Fig. 4-4   The band gap as function of PH$_3$ to SiH$_4$ ratio

4.3 a-Si:H / a-Si:H Tandem Solar Cell

The structure of an a-Si:H / a-Si:H tandem solar cell was shown in Fig. 4-5. The cells were made on SnO$_2$:F coated glass with a superstrate configuration, and the thickness of each layer is also in the figure. The tandem solar cell consists of a cell with a thinner i-layer on the TCO side and a cell with thicker i-layer on metal electrode side. To resist the boron diffusion and improve current extraction, a buffer layer between p- and i-layer is used in both cells. The interface between top and bottom cell (or between n-type and p-type a-Si:H) which is known as TRJ. The structure of such tandem solar cell would be the standard for the following experiment. Besides, the performance of a-Si:H single junction solar cell which the i-layer thickness is 360 nm is shown in Fig. 4-6.
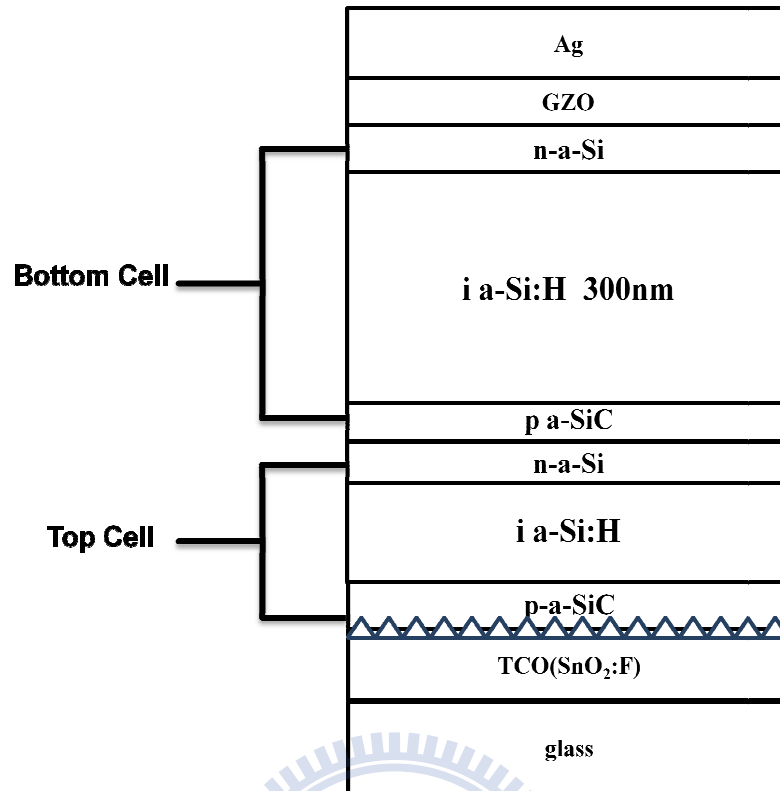
Fig. 4-5   Schematic of an a-Si:H / a-Si:H tandem solar cell
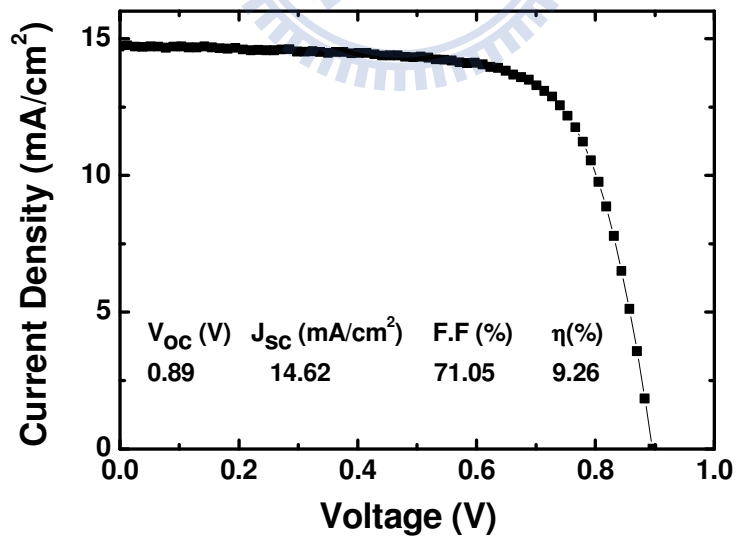
Fig. 4-6   The I-V characteristics of a-Si:H single junction solar cell with the

same i-layer thickness

4.3.1 Current Matching between Top and Bottom cell – optimization of the thickness of i-layer in the top cell

In this device structure, the top cell and bottom cell are connected in series. According to the current limiting phenomenon, the lower current generated from the top or bottom cell would dominate the current of the tandem solar cell. In order to obtain the best solar cell efficiency, the photo-generated current of top cell must be matched to that of bottom cell. If the current matching is properly made, the initial efficiency of the a-Si:H / a-Si:H tandem cell is approximately equal to the efficiency of the single junction cell with the same i-layer thickness. Most important of all, the light-induced degradation will be decreased.

The creation of the additional defects in the intrinsic layer due to the Stabler-Wronski effect deteriorates the collection of carriers by decreasing their lifetime and also distorts the electric field. For single junction a-Si:H solar cell, the optimal thickness of the intrinsic layer is in the range of 250 nm to 320 nm [58]. In this section, the i-layer thickness of the top cell was varied while the i-layer thickness of the bottom cell is fixed at 300 nm. The results of η, F.F, J_{sc} and V_{oc} are in Fig. 4-7. The F.F. and V_{oc} show no obvious change in this experiment. However the i-layer thickness of top cell has the most impact on the J_{sc} in which the maximum and minimum values are 6.27 mA/cm^2 and 5.43 mA/cm^2 respectively. Due to the significantly change in J_{sc}, the efficiency shows the same tendency in Fig. 4-7. The highest efficiency is 6.6 % when the thickness of top cell is 60 nm. Some groups have reported the results of the optimized thicknesses of top and bottom cell for current matching. Von der Linden et al. [59] have found an optimal ratio between the i-layer thickness of the top and bottom cell of 1:6 in a-Si:H / a-Si:H modules. Y. Ichikawa et al. [60]   obtained the highest initial efficiency 12.0 % when the thicknesses of top and bottom cell were 70 nm and 300 nm, respectively. Fig. 4-8 shows the i-layer

thickness dependent I-V characteristics of the top cell, the improvement of J_{sc} is achieved by current matching. In order to investigate the current matching thoroughly between top and bottom cell, the quantum efficiency of tandem cell is shown in Fig. 4-9.

Fig. 4-7 The efficiency, F.F., J_{sc} and V_{oc} of the tandem cell as function of the i-layer thickness of the top cell
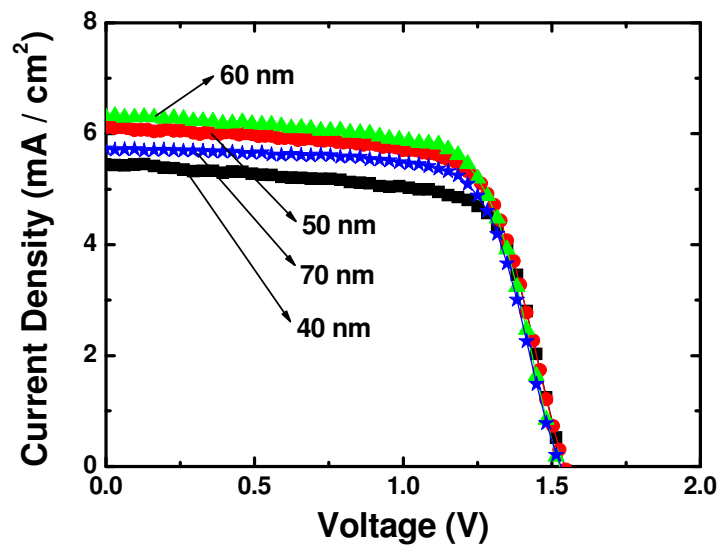
Fig. 4-8   The I-V characteristics of a-Si:H / a-Si:H tandem solar cells with

different i-layer thickness of the top cell

Table. 4-1   The perfoemance of of a-Si:H / a-Si:H tandem solar cells with

different i-layer thickness of the top cell

t (nm)	V_{oc} (V)	J_{sc} (mA/cm^2)	F.F. (%)	η (%)
40	1.54	5.43	69.84	5.84
50	1.54	5.92	67.88	6.39
60	1.53	6.27	68.79	6.60
70	1.52	5.73	71.17	6.21
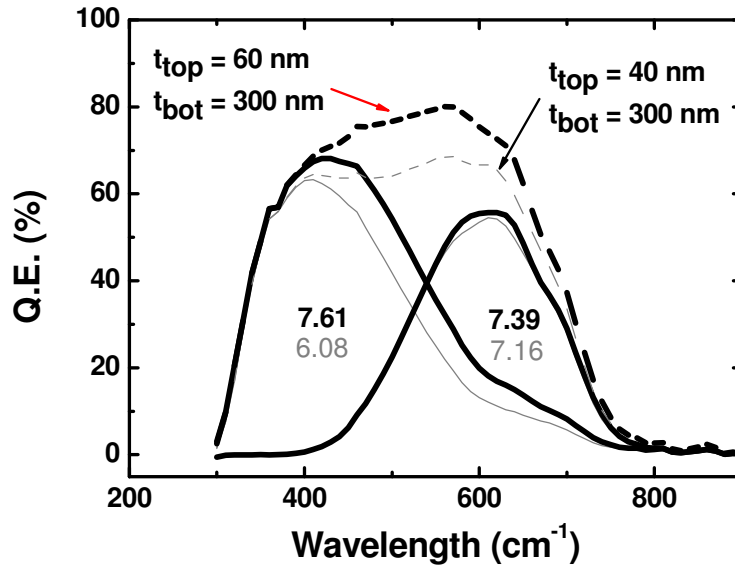
Fig. 4-9   Quantum efficiency with i-layer thickness of 40 nm and 60 nm of the

top cell

4.3.2 Effect of n-layer Thickness on the Performance of Tandem Solar Cell

The TRJ is a critical issue to improve the current recombination between the top and bottom cell. The thickness of both n-layers in the previous section is 30 nm which is the same thickness of referential a-Si:H single junction solar cell. In order to prevent light absorption in the n-layer which also means to increase absorption in i-layer at the same time, the thickness of n-layer in top cell was reduced from 30 nm to 5 nm. It can be seen in Fig. 4-10 that the J_{sc} shows a significant increase with reduction in n-layer thickness. The J_{sc} can reach to 7.18 mA/cm^2 by reducing light absorption in n-layer. However, the V_{oc} decreases suddenly when the top n-layer thickness decreases from 10 nm to 5 nm. This phenomenon may be due to the depletion region between the TRJ overlaps the depletion of n-layer of top cell, and the built-in voltage of top cell is weaken by this interference. This can also be proven by the decreasing in F.F. decreases from 68.79 % to 61.27 % with decreasing thickness.

In Fig. 4-11, the shunt resistance clearly decreases when the top n-layer thickness is 5 nm.
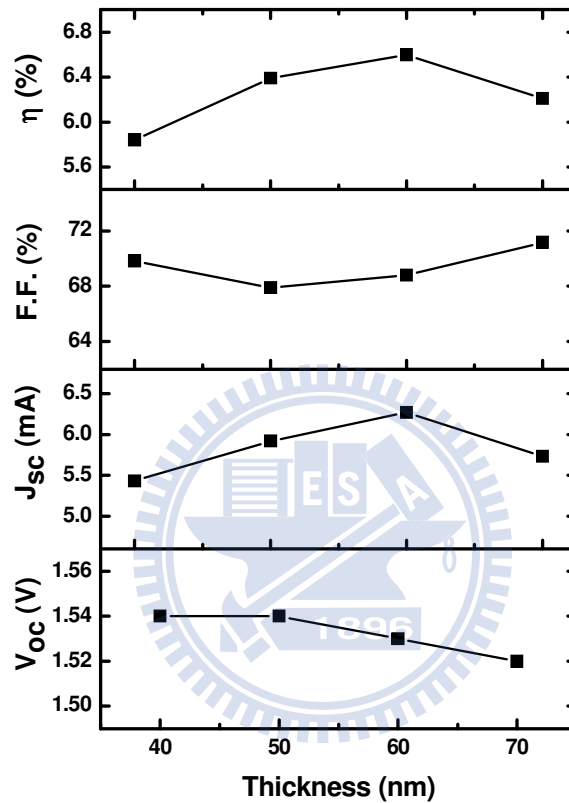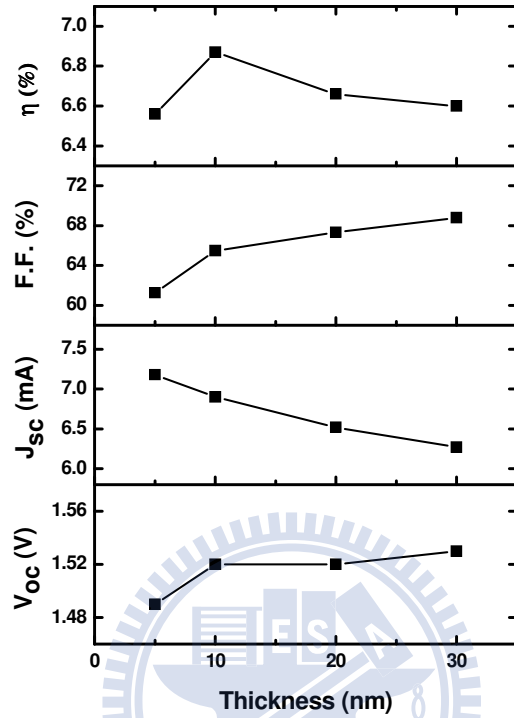

Fig. 4-10   The efficiency, F.F., J_{sc} and V_{oc} of the tandem cell as function of the

n-layer thickness of top cell
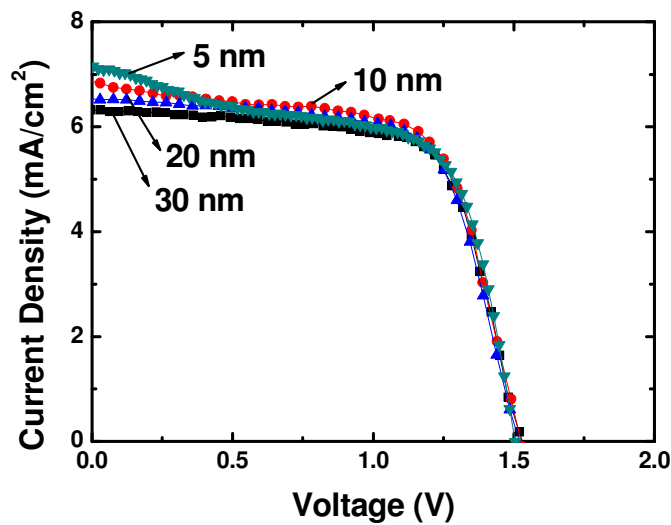
Fig. 4-11   The I-V characteristics of a-Si:H / a-Si:H tandem solar cells with

different n-layer thickness of top cell

Table. 4-2   The performance of a-Si:H / a-Si:H tandem solar cells with different

n-layer thickness of top cell

t (nm)	V_{oc} (V)	J_{sc} (mA/cm^2)	F.F. (%)	η (%)
5	1.49	7.18	61.27	6.56
10	1.52	6.90	65.48	6.87
20	1.52	6.52	67.33	6.66
30	1.53	6.27	68.79	6.60

The n-layer thickness of the bottom cell is also a parameter needed to be optimized in this structure. The thickness of the n-layer in top cells was fixed at 10 nm in this section. In Fig. 4-13, J_{sc} and V_{oc} show lightly change by modulating n-layer thickness. The cell efficiency increased from 6.87 % to 7.05 % because of the increase in F.F. and V_{oc} by reducing n-layer thickness.
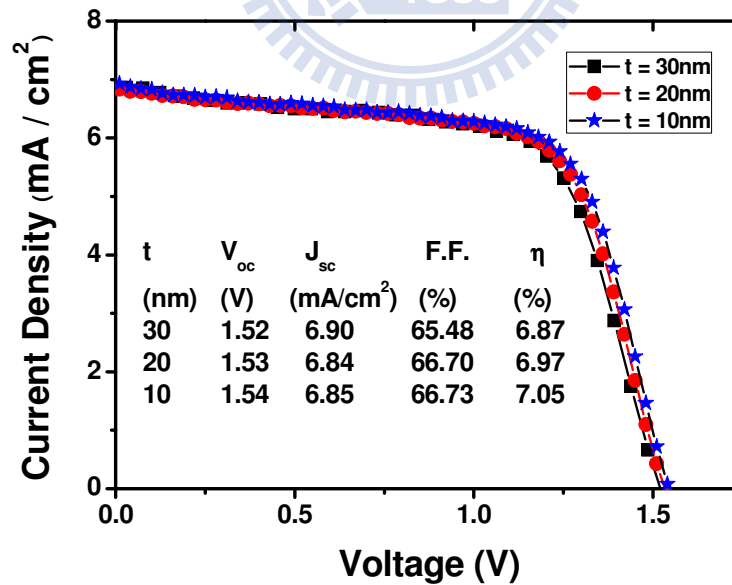
Fig. 4-12   The I-V characteristics of a-Si:H / a-Si:H tandem solar cells with

different n-layer thickness of bottom cell

In Fig. 4-12, these three I-V curves are almost the same, and just a slightly different on series resistance. Reducing bottom n-layer thickness could possible decrease the series resistance of device, so the F.F. increases slightly.

Fig. 4-13 The efficiency, F.F., J_{sc} and V_{oc} of the tandem cell as function of the n-layer thickness of top cell

## 4.3.3 Effect of Improving Buffer Layer

It had been reported that band-gap profiling of the p / i interface improve the efficiency of a-Si:H single junction solar cell [61-62]. In the standard structure mentioned above, it has only one a-SiC:H thin film between the p-layer and i-layer. The result of I-V measurement between two different buffer layers in a-Si:H / a-Si:H tandem solar cells is in Fig. 4-14. The grading buffer layer has twice the thickness than standard configuration which was optimized in a-Si:H single junction solar cell.

It can be seen in Fig. 4-14 that the improved buffer increases the V_{oc}. However, the J_{sc} with improved buffer is lower which is not the result we expected. The following experiment would investigate the effect of the improved buffer.
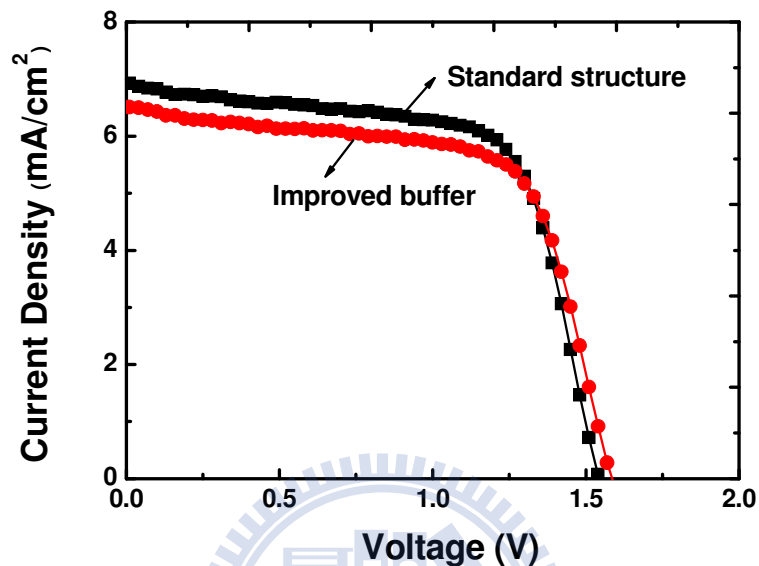
Fig. 4-14   The I-V characteristics of a-Si:H / a-Si:H tandem solar cells with different buffer layer

The previous experiment was meant to introduce an improved buffer to further increase the current extraction from the intrinsic layer. However, the results were not as good as expected. This should be arising from the deviation of the current matching between the top / bottom cells with new buffer. In the following experiments we fine tune the i-layer thickness of the top cell. As can be seen in Fig. 4-15, the V_{oc} has no significant change with different thickness in which the same result in Fig. 4-7 is shown. On the contrary, J_{sc} effectively increase from 5.86 mA/cm^2 to 7.05 mA/cm^2. Compare to the cells prepared with the standard buffer, the optimized efficiency shifted toward a thicker i-layer thickness of the top cell. The improved buffer shows an ability of effective current transportation. In Fig. 4-16 shows the same result of

increasing J_{sc} by current matching.

In a-Si:H single junction solar cell, buffer grading improves the current transport from i-layer to p-layer due to band-gap profiling. Because of this improvement of J_{sc}, the thickness of top cell should be larger to match the current of bottom cell which the absorption is larger due to a much thicker intrinsic layer. The F.F. increased with thicker i-layer thickness of top cell.
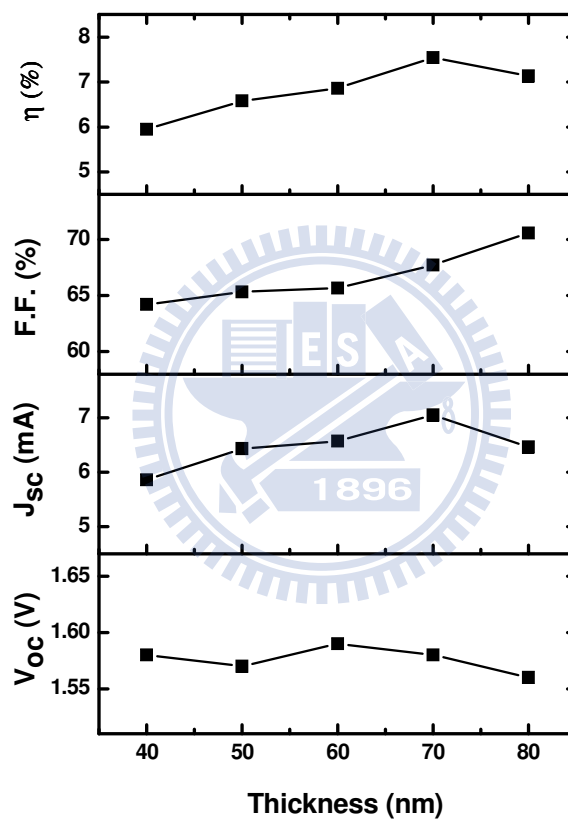
Fig. 4-15   The efficiency, F.F., J_{sc} and V_{oc} of the tandem cell as function of the
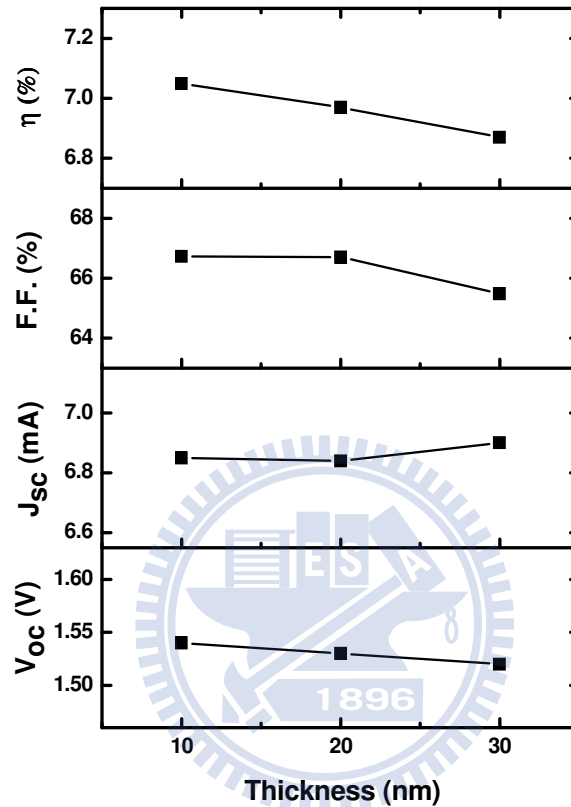
i-layer thickness of top cell
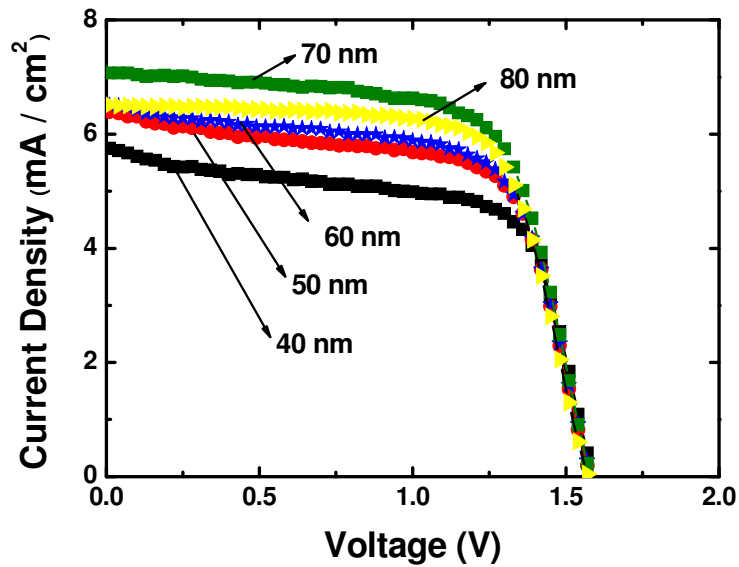
Fig. 4-16   The I-V characteristics of a-Si:H / a-Si:H tandem solar cells using improved buffer with different i-layer thicknesses of the top cell

Table. 4-3   The performance of a-Si:H / a-Si:H tandem solar cells using improved buffer with different i-layer thicknesses of the top cell

t (nm)	V_{oc} (V)	J_{sc} (mA/cm^2)	F.F. (%)	η (%)
40	1.58	5.86	64.20	5.95
50	1.57	6.43	65.32	6.58
60	1.59	6.57	65.66	6.86
70	1.58	7.05	67.72	7.54
80	1.56	6.46	70.55	7.13

4.3.4 μc-Si n-layer in Tunneling Recombination Junction

The TRJ plays an important role to obtain the optimal efficiency of tandem solar cell. It has to be an ohmic and low resistive connection between the top and bottom

cell, and also has low optical absorption in the region. µc-Si:H seems to be an appropriate material in this junction because of its low mobility gap which is beneficial to recombination and low optical absorption than a-Si:H. The detail parameters for the deposition of µc-Si:H n-layer is listed in Table. 2-1. In order to crystallize in such a thin thickness (20 nm), the high dilution ration and low pressure was required. A high rf power should work but would lead to serious ion bombardments, therefore, we chose an appropriate value to avoid damaging a-Si:H thin film. The deposition rate is 0.057 nm / s. Compared to a-Si:H, the properties of the µc-Si:H film are greatly affected by the crystallinity which not only depends on deposition parameters, film thickness but also the substrate. In order to investigate the practical crystallinity of µc-Si:H n-layer on an amorphous surface, we deposited 20 nm a-Si:H thin film on SnO_2:F coated thick glass then started to deposit the µc-Si:H thin film.

Table. 4-4 Deposition conditions of µc-Si:H n-layer

Parameter	Value
T_{sub} (^{o}C)	200
Pressure (torr)	1.88
Power (W)	220
$[H_2]$ / ($[H_2]$ + $[SiH_4]$) (%)	99.5
E / S (mm)	14
Thickness (nm)	200

Fig. 4-17 shows the Raman spectrum of two different thicknesses of µc-Si:H. The peak at 520 cm^{-1} is not obvious for the 20 nm-thick µc-Si:H n-layer but turned

into sharp when the thickness increase to 100 nm. Although the crystallinity of the 20 nm-thick μc-Si:H appears as quite low, it should be in fact much higher for the individual μc-Si:H film. This is due to the signal from the a-Si:H unlayer which even contributes more than μc-Si:H due to the higher coefficient of absorption of a-Si:H.
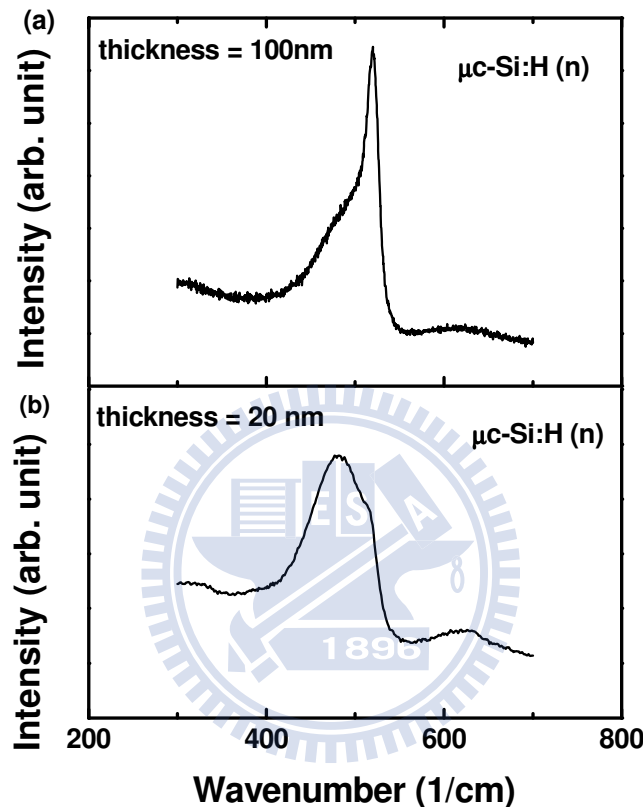
Fig. 4-17   Raman spectrum of μc-Si:H n-layer with different thickness of (a) 100 nm and (b) 20 nm

The I-V characteristic of three different TRJ is shown in Fig. 4-18. The structure of these three cells is the standard structure without the improved buffer. The black square in the figure represents the I-V result with TRJ which replaced the a-Si:H n-layer by μc-Si:H n-layer. The star and circle are the TRJ with thicknesses of a-Si:H n-layer. The red circle one shows an S-shape problem in light I-V measurements, and this problem occurs in all the cells before except the TRJ of 5 nm a-Si:H n-layer. The reason for S-shape problem is that n-layer and p-layer in TRJ result in a diode in

reverse direction against the top and bottom cell, as shown in Fig. 4-19. This diode in reverse direction would resist the photo-generated current in tandem solar cell. J. Loffler, et al [38] had found the S-shape problem in TRJ of a-Si:H n-layer and μc-Si:H p-layer, because the incubation layer of μc-Si:H p-layer lead to the actual interface is formed by a-Si:H n-layer and a-Si:H p-layer.

The TRJs of μc-Si:H n-layer and 5 nm a-Si:H n-layer has no S-shape problem, but the efficiency decrease significantly.
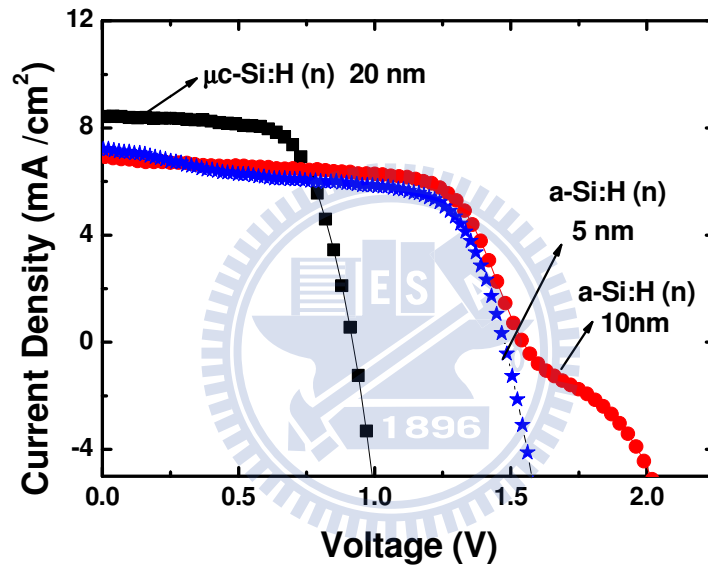
Fig. 4-18   The I-V characteristics of a-Si:H / a-Si:H tandem solar cells with different n-layer in TRJ
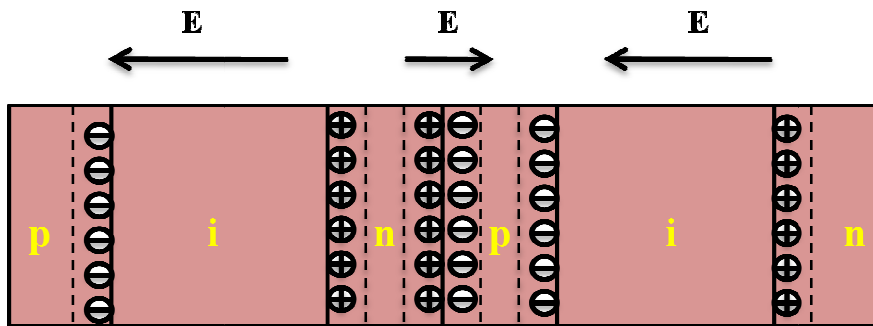
Fig. 4-19   The space charge region, the depletion region and the electric field in a-Si:H / a-Si:H tandem solar cell

4.4 Deposition and Characterization of μc-Si:H i-layer

For a better spectral response to achieve higher efficiency of the solar cell, a micromorph tandem solar cell was proposed [58]. A micromorph solar cell has a top cell with a-Si:H and a bottom cell with μc-Si:H. In this study, the deposition and characterization of the μc-Si:H thin film was carried out to figure out a suitable material for solar cell application.

In this chapter, we study the effect of substrate temperature, total flow rate, rf power and hydrogen dilution ratio on the characteristics of μc-Si:H. Because the high pressure depletion region mentioned above, the pressure is set in 6torr. In this high pressure deposition condition, the collision between radical is more often so the free mean path of radical is decreased. To avoid gas phase reaction and powder formation, the distance between electrode and substrate is set in 7 mm.

Table. 4-5　Deposition conditions of μc-Si:H by PECVD

Parameter	Value
T_{sub} (^{o}C)	200
Pressure (torr)	6
Power (W)	100~600
$[H_2] / ([H_2] + [SiH_4])$ (%)	95.24~98.77
E / S (mm)	7
Thickness (nm)	300~600

4.4.1 Influence of Substrate Temperature

Substrate temperature (T_{sub}) is the basic and most important parameter which we should consider first before depositing μc-Si:H. In this study, we used thermal couple

to measure substrate temperature. Fig. 4-20 shows the temperature profile of the T_{sub} in a deposition process. The substrate was first transferred into the reaction chamber, and then the T_{sub} reached to a saturation temperature at ~179 ^{o}C in vacuum. Around the 13th minute, we began to flow hydrogen into the reaction chamber and maintaining at a certain high pressure. As a result, the T_{sub} suddenly rose because of the heat conduction from the heater. After the hydrogen flow, the heater temperature decreased 10 ^{o}C in 10 minutes due to the high flow rate and high pressure which carried the heat away from the substrate. As a result, the T_{sub} decreases to 183 ^{o}C. In practical situation, the higher plasma power used for μc-Si:H compare to a-SiH, cause the substrate to heat up during film deposition [63]. The substrate temperature is probably greater than the temperature we estimated, but it is still an appropriate region to deposit μc-Si:H thin film.

The high flow rate with high pressure conduct heat away from heater, so the heater temperature decrease with the hydrogen flow. At the same heater temperature, the T_{sub} in μc-Si:H deposition condition would lower than the condition in a-Si:H. Vetteral et al. [64] and Nasuno et al. [65] observed a deterioration of μc-Si:H solar cell efficieny at $T_{sub} > 200$ ^{o}C for p-i-n cell, and this deterioration was not happen for n-i-p cell. It was because of an enhanced diffusion of boron from p-layer to i-layer.
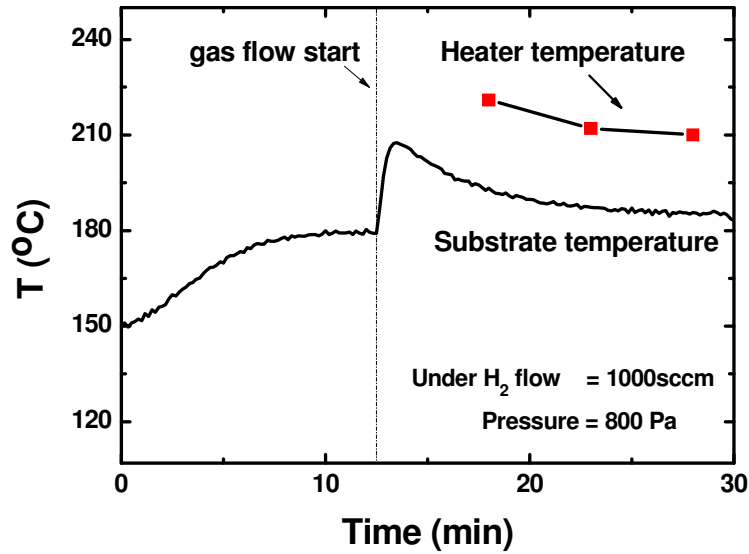
Fig. 4-20   Substrate temperature measurement at 6 location on substrate

by thermal couple

4.4.2 Influence of Total Flow Rate

In industrial production, the total gas flow is a significant parameter to reduce cost by reducing gas consumption. But in our PECVD system, the minimum total flow rate (~800 sccm) is needed to maintain high pressure during deposition. Besides, the total flow rate determines the residential time of gas molecules, which is estimated in room temperature by

$$t_{res} = \frac{V \times P_{dep}}{f_{total} \times P_0} = \frac{A \times d_{el} \times P_{dep}}{f_{total} \times P_0} \qquad [66]$$

where A is the substrate area; d_{el} is the distance between electrode and substrate; P_0 is the standard pressure (1013 hpa).

In order to study the influence of total flow rate, other parameters were fixed ($T_{sub} = 200^oC$; Power = 200 W; Pressure = 6 torr ; $[H_2] / ([SiH4] + [H_2]) = 97.56 \sim 94.67$). Two total flow rate of 800 sccm and 1500 sccm were conducted. The total flow rate strongly affects the deposition rate even in the same hydrogen dilution ratio,

as shown Fig. 4-21. This should be due to more SiH_4 molecules were dissociated by the plasma. Although the total flow rate increased from 800 sccm to 1500 sccm, the deposition rate did not increase proportional to the total flow rate. It implies that SiH_4 molecules reach to a saturation at the same rf power, therefore, the gas utilization is much lower at high total flow (1500 sccm) than low total flow (800 sccm).
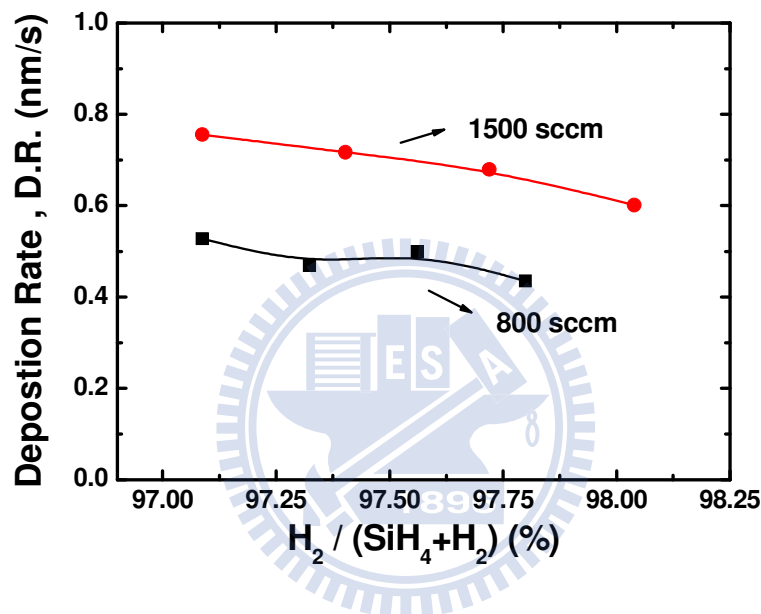
Fig. 4-21   Deposition rate as a function of hydrogen dilution ratio with different total flow rate

The crystallinity as a function of hydrogen dilution ratio with the two total flow rates is shown Fig. 4-22. The condition of higher total flow has lower crystallinity which may be due to the higher deposition rate. Because the deposition rate is high at high flow rate, the precursors do not have sufficient time to diffuse to appropriate sites to form crystallites.
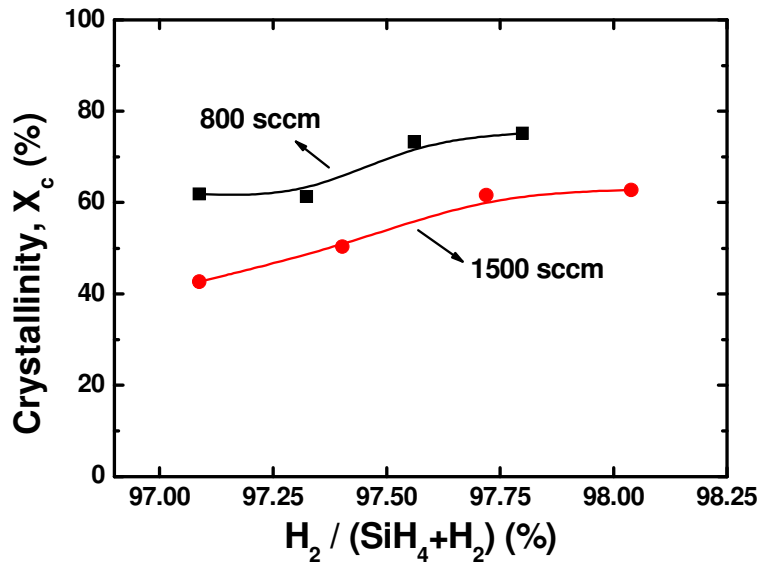
Fig. 4-22 Crystallinity as a function of hydrogen dilution ratio with different

total flow rate

4.4.3 Influence of RF-Power

The deposition of μc-Si:H is usually at a high power condition, except in a VHF PECVD system. The high frequency in VHF system leads to high electron density which makes it possible to obtain a higher deposition rate. However, this might lead to a film with lower quality [67-68].

It has been mentioned that SiH_4 depletion is required to improve film quality, so an optimum power is essential for μc-Si:H deposition. As can be seen in Fig. 4-23, rf power is varied from 100 W to 600 W while other parameters is fixed (Ts = 200°C; Pressure = 6 torr; [H$_2$] / ([SiH4] + [H$_2$]) = 96.39).As the rf power is lower than 200 W, the crystallinity dramatically decreased to 0 with the decreasing power. This suggests that at such low power, the atomic hydrogen etching becomes insufficient to form crystallites and only amorphous phase is deposited. When the power exceeds 200 W, the crystallinity stays a constant value which may indicate that the gases introduced were effectively dissociated. From the point that higher power has more

ion-bombardment which may introduce more damage, the power at about 200 W is appropriate for crystallization with lower defects.
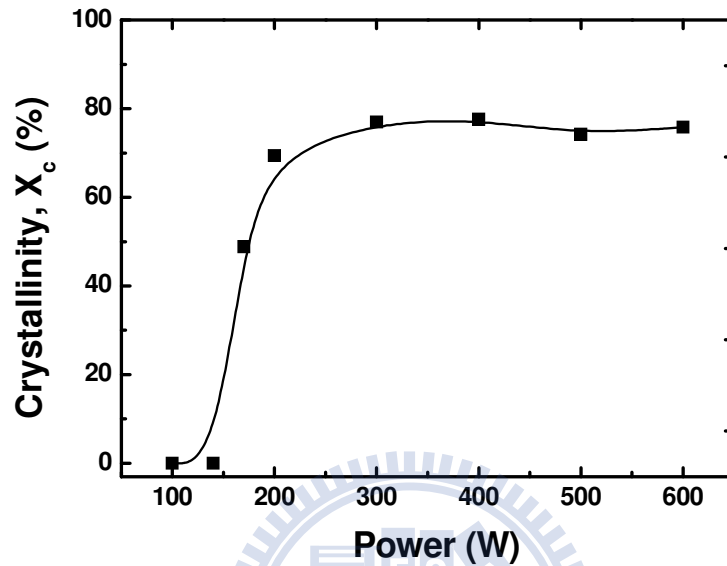
Fig. 4-23　Crystallinity as a function of power

As shown in Fig. 4-24, the deposition rate increases when the power increases from 100 W to 600 W. It is because the rising power lead to higher SiH_4 dissociation. However, the deposition rate does not rise proportionally as much as the power. One reason of this phenomenon is that the SiH_4 depletes, and the source gas is not enough to support further deposition. Another is the hydrogen etching effect being stronger while the power increase which removes the part of the deposited material.
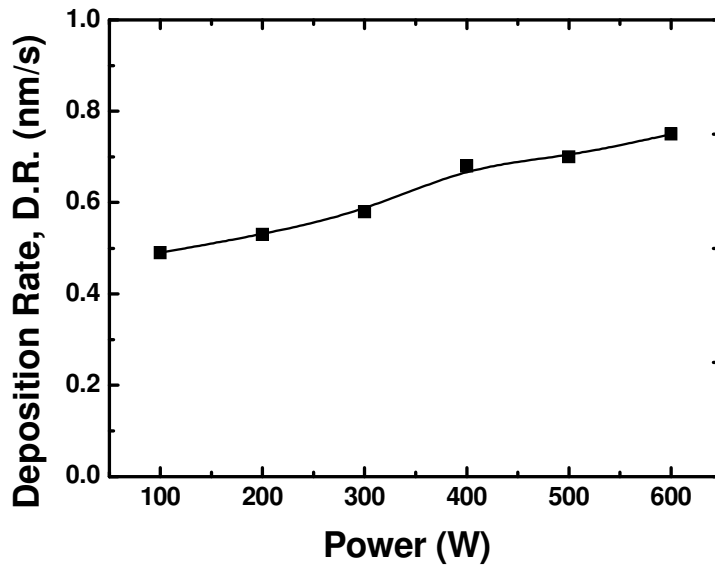
Fig. 4-24   Deposition rate as a function of power

In order to understand more about the microcrystalline structure, the XRD analysis of μc-Si:H layers deposited with power varying from 200 W to 600 W are shown in Fig. 4-25. Two main diffraction peaks corresponding to the (111) and (220) silicon crystallographic planes are indicated. . Crystallographic growth of the μc-Si:H in (220) orientation increases when power increased. If the (220) peak intensity is much higher than the (111) peak intensity, it would indicate a preferred (220) orientation for the μc-Si:H. But this is not obviously in this series. The (220) preferential orientation is frequently observed in device grade material [69]. In Fig. 4-25 , the peak intensity of (111) orientation increase while power is increased from 200 W to 600 W. But the peak of (220) orientation which preferred in device is decreasing.
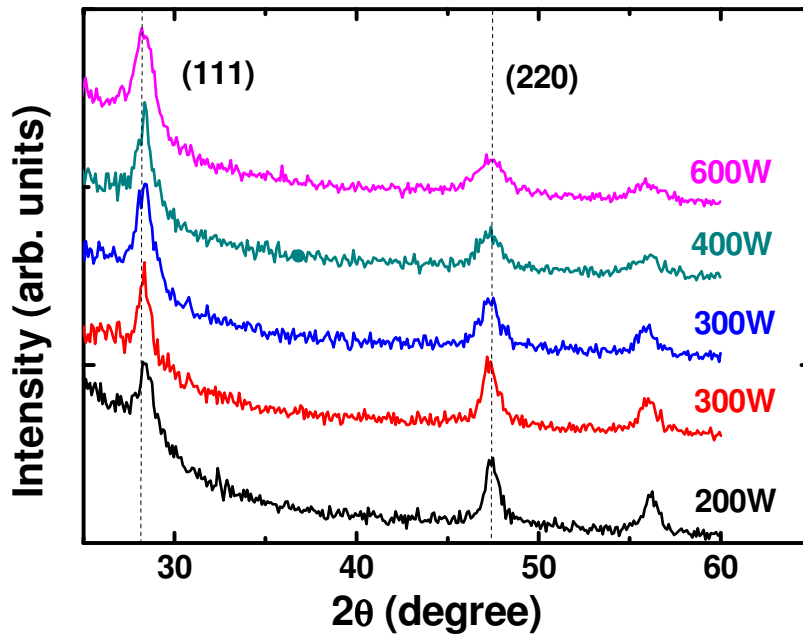
Fig. 4-25   XRD spectra obtained for a series of μc-Si:H layers deposited on glass substrates at various powers

In Fig. 4-26, we use (220) / (110) as an parameter to compare the μc-Si:H. The figure shows that the power significantly affects the orientation of μc-Si:H. The (220) / (111) ratio drastically decrease while the power increase from 200W to 600W. This shows that the low power is preferred to deposit μc-Si:H in (220) orientation. E.Vallat-Sauvain et al. [69] observed that the (220) orientation occurred obviously in a-Si:H to μc-Si:H phase transition. In this series, the crystallinity of all samples are around 60 %~80 %. When the power decrease to 100 W, and the sample turn out to be all amorphous phase. Although the a-Si:H to μc-Si:H phase transition cannot be observed in Fig. 4-26, it shows the same trend that the ratio (220) / (110) increase while the deposition condition close to the transition region. In this experiment, a better (220) to (110) ratio appears when the power is 200 W.
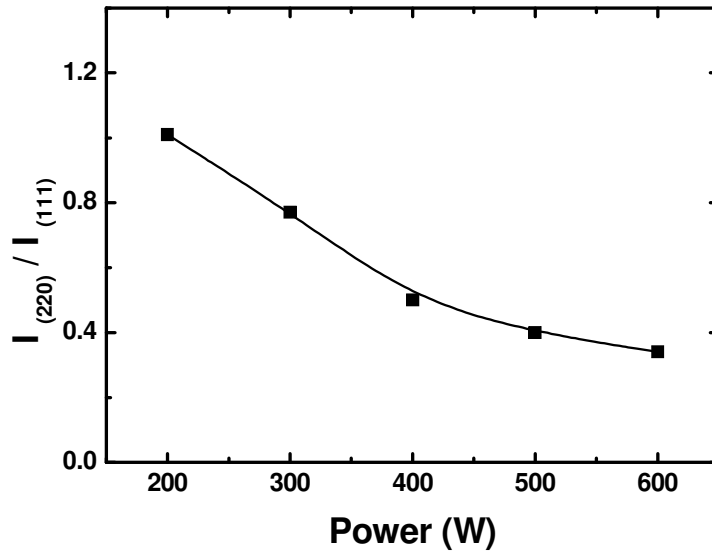
Fig. 4-26   The ratio (220) / (111) as a function with varying power

Because the hydrogen dilution ratio we used in the previous series is too low to crystallize at a power of 100 W, other experiment was conduct to find the optimum power. As shown in Fig. 4-27, there are three series of varying hydrogen dilution ratio at different power. According to the result in Fig. 4-26 which lower power is preferred for (220) orientation, higher hydrogen dilution ration at power of 100W was chose to ensure crystallization. For the power of 300W and 400W, the crystallinity is around 70 %~85 %. The ratio of (220) / (110) at 300W is slightly higher than power of 400 W. The highest ratio of (220) / (110) occurs with hydrogen dilution ratio 97.56 % at power of 100W. The crystallinity at this point is 53 %, which is in the transition region. The relation between the ratio (220) / (110) and hydrogen dilution ration would be studied in the next section.
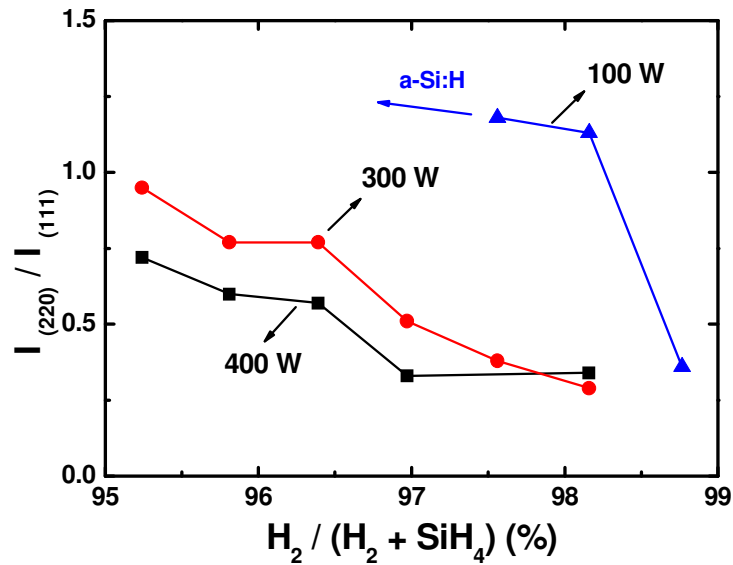
Fig. 4-27   The ratio (220) / (111) with different power

4.4.4 Influence of Hydrogen Dilution Ratio

Due to the result of power optimization, the power of this series is fixed at 100W to study the effect of hydrogen dilution ratio. Many studies indicate that the best solar cell efficiency is obtained at X_c = 50%, and varying hydrogen dilution ratio is a fast and directed method to control the crystallinity. In Fig. 4-28a, the crystallinity increase with hydrogen dilution ratio, and the transition between a-Si:H and μc-Si:H occurs when hydrogen dilution ratio is 97 %~98 %. In surface growth models mentioned above that μc-Si:H nucleation is due to the enhanced surface diffusion of SiH_3 radicals from the coverage of surface by hydrogen [28]. This enhanced surface mobility lead to the incorporation of silicon into sites of minimum energy and form stable crystallites. Moreover, selective etching of the amorphous phase by atomic hydrogen has also been considered. To study the electric property of μc-Si:H, σ_{ph} and σ_d is shown in Fig. 4-28b. The red square and black square correspond to σ_{ph} and σ_d, and the blue circle is photosensitivity. We can observe that σ_d drops by several orders of magnitude to 10^{-10} Scm^{-1}, which is the typical value of a-Si:H. σ_{ph} shows an slightly

increase with increasing crysrallinity, because the transition to µc-Si:H which has the higher conductivity to transfer photo-generated current. It has been report that and the highest photosensitivity for µc-Si:H close to the transition of amorphous growth.

It has been reported that µc-Si:H often shows high σ_d and the Fermi level position is lifted toward conduction band side [70]. This n-type character has been ascribed to oxygen related donors in µc-Si:H probably at grain boundary [70-71]. It also has been show that the n-type character decreases the spectral respond in long wavelength region and increases the shunt leakage current which probably decreases the V_{oc} in solar cell device. In high crystallinity region, the high defect density leads to a reduction of the photo-generated carrier lifetime which causes the low photosensitivity.

The deposition rate of this series is shown in Fig. 4-29. The deposition rate decrease with increasing hydrogen dilution ratio, and there is no obvious difference on the hydrogen etching effect between a-Si:H and µc-Si:H. However, the deposition rate is not high in this series.
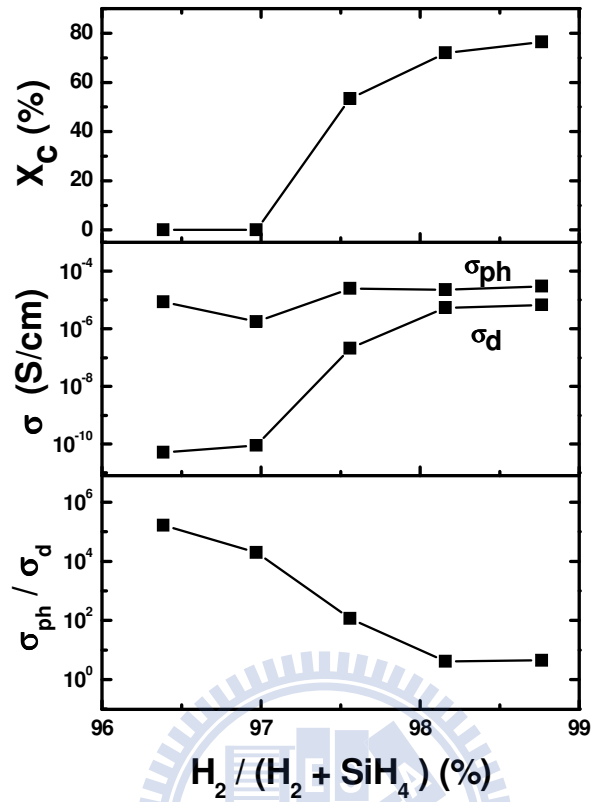
Fig. 4-28   Crystallinity,photo- and dark conductivity as a function of hydrogen
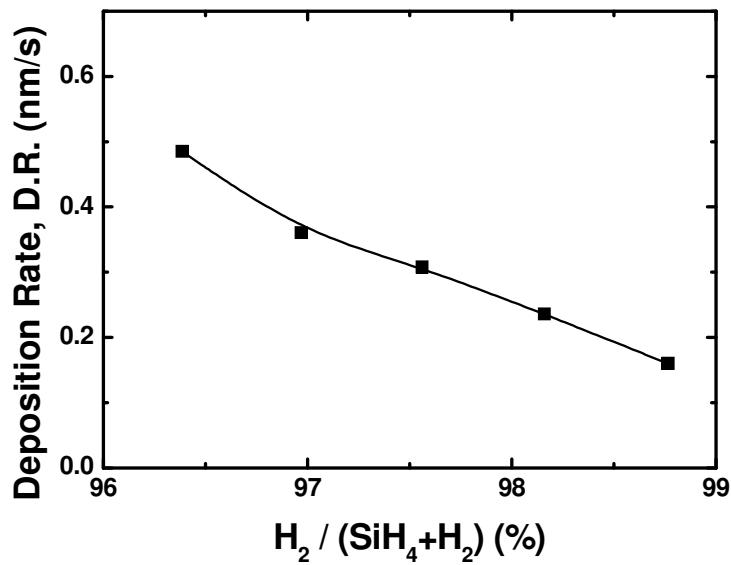
dilution ration

Fig. 4-29   Deposition rate as a function of hydrogen dilution ration

57

The ratio (220) / (111) with varying hydrogen dilution ratio is in Fig. 4-27. These three series with different powers show the same trend that the ratio increases with increasing hydrogen dilution ratio. And highest ratio is also observed at a-Si:H to μc-Si:H phase transition which is the same region observed in the series with varying power.

In summary, the maximum value of ratio (220) / (111) is obtained at the transition region between a-Si:H and μc-Si:H. this result shows on the two series of varying power and varying hydrogen dilution ratio. We think it is the right direction to yield a high efficiency μc-Si:H solar cell at the transition region. Due to the equipment problem, we cannot deposit a μc-Si:H single junction cell to prove this assumption.

Chapter 5   CONCLUSIONS

a-Si:H / a-Si:H tandem solar cells are prepared in an radio-frequency (27.12 MHz) PECVD multi-chamber system. The current matching between top and bottom cell is a crucial part to improve J_{sc}. The J_{sc} increase from 5.43 mA to 6.27 mA by optimizing the i-layer thickness of top cell. Using band-gap profiling method in buffer layer, the optimal thickness of top i-layer shift to 70 nm to achieve current matching. The J_{sc} increased to 7.05 mA with improved buffer. Beside, the V_{oc} also increases from 1.58 to 1.54 due to the increase of buffer layer thickness when the improved buffer is applied. The highest a-Si:H / a-Si:H tandem solar cell efficiency of 7.58% is obtained with improved buffer. In this study, μc-Si:H is applied in TRJ, and the I-V characteristic shows no effect of reverse electric field against the built-in voltage of top and bottom cell, but the V_{oc} decrease significantly from ~1.55 V to 1 V.

μc-Si:H thin films have been developed in an radio-frequency (27.12 MHz) PECVD multi-chamber system under different total flow rate, rf powers, and hydrogen dilutions ratio. Finding an appropriate T_{sub} is the prior thing to deposit μc-Si:H thin films. Due to the high pressure and high flow rate compared with the parameters of a-Si:H thin film deposition, the T_{sub} is lower during the μc-Si:H deposition process. To avoid ion bombardment during the deposition, the lower power (100W) is used in this study and the peak of (220) orientation is also obvious under the lower deposition power. The crystallinity is 53.4 % when the hydrogen dilution ratio is 97.56 % and the photosensitivity and the ratio of (220) / (111) achieve to optimal value 10^2 and 1.1 respectively. In conclusion, low power and the deposition condition close to transition region are preferred to deposit μc-Si:H in (220) orientation. In conclusion, the transition region from a-Si:H to μc-Si:H shows a good material characteristic both in XRD measurement and photosensitivity.

Chapter 6　FUTURE WORKS

In a-Si:H / a-Si:H tandem solar cell structure, the same improved buffer is used in both top and bottom cell. Due to the different thickness of top and bottom cell, the optimal thickness and bandgap profiling of improved buffer should be adjusted individually for each cell. Besides, the μc-Si n-layer used in TRJ solves the S-shape problem, but the cell efficiency decrease significantly to 4.95%. There are some reasons might cause this situation, the gas doping ratio of μc-Si:H n-layer is twice than a-Si:H p-layer, so the depletion region would shift to the a-Si:H p-layer which the thickness is only 8nm. This thickness may not thick enough for this increased depletion region, and the built-in voltage of bottom cell would also be reduced. Therefore, increasing thickness of a-Si:H p-layer could be one solution, but the light absorption should be considered in this situation. Howe ever, the μc-Si:H p-layer can also applied in TRJ for the following experiments.

In order to deposit micromorph solar cell, μc-Si:H single junction solar cell is the essential part to study. The best crystallinity and (220) orientation of μc-Si:H i-layer for cell efficiency is not verified now. Moreover, the research of μc-Si:H single junction solar cell structure, like μc-SiC p-layer can be applied to reduce light absorption.

REFERENCE

[1]   I. Repins, M. Contreras, B. Egaas, C. DeHart, J. Scharf, C. Perkins, B. To, and R. Noufi, "Short Communication: Accelerated Publication 19P 9%-efficient ZnO/CdS/CuInGaSe2 solar cell with 81¡P 2% fill factor," *Progress in Photovoltaics: Research and Applications,* vol. 16, pp. 235-239, 2008.

[2]   H. Chen, J. Hou, S. Zhang, Y. Liang, G. Yang, Y. Yang, L. Yu, Y. Wu, and G. Li, "Polymer solar cells with enhanced open-circuit voltage and efficiency," *Nature Photonics,* vol. 3, pp. 649-653, 2009.

[3]   K. Yamamoto, A. Nakajima, M. Yoshimi, T. Sawada, S. Fukuda, T. Suezaki, M. Ichikawa, Y. Koi, M. Goto, and T. Meguro, "A thin-film silicon solar cell and module," *Progress in Photovoltaics: Research and Applications,* vol. 13, pp. 489-494, 2005.

[4]   A. Shah, H. Schade, M. Vanecek, J. Meier, E. Vallat-Sauvain, N. Wyrsch, U. Kroll, C. Droz, and J. Bailat, "Thin-film silicon solar cell technology," *Progress in Photovoltaics: Research and Applications,* vol. 12, pp. 113-142, 2004.

[5]   R. Street, *Hydrogenated amorphous silicon*: Cambridge Univ Pr, 1991.

[6]   J. Poortmans and V. Arkhipov, *Thin Film Solar Cells Fabrication, Characterization and Applications*: John Wiley & Sons Ltd, 2006.

[7]   S. Guha, K. Narasimhan, and S. Pietruszko, "On light induced effect in amorphous hydrogenated silicon," *Journal of Applied Physics,* vol. 52, p. 859, 1981.

[8]   S. Sriraman, S. Agarwal, E. Aydil, and D. Maroudas, "Mechanism of hydrogen-induced crystallization of amorphous silicon," *Nature,* vol. 418, pp. 62-65, 2002.

[9]   K. Nomoto, Y. Urano, J. Guizot, G. Ganguly, and A. Matsuda, "Role of hydrogen atoms in the formation process of hydrogenated microcrystalline silicon," *Japanese Journal of Applied Physics,* vol. 29, 1990.

[10]   M. Katiyar and J. Abelson, "Investigation of hydrogen induced phase transition from a-Si: H to [mu] c-Si: H using real time infrared spectroscopy," *Materials Science and Engineering A,* vol. 304, pp. 349-352, 2001.

[11]   N. Layadi, P. Roca i Cabarrocas, B. Drevillon, and I. Solomon, "Real-time spectroscopic ellipsometry study of the growth of amorphous and microcrystalline silicon thin films prepared by alternating silicon deposition and hydrogen plasma treatment," *Physical Review B,* vol. 52, pp. 5136-5143, 1995.

[12]   J. Bertomeu, "The role of hydrogen in the formation of microcrystalline silicon," *Materials Science and Engineering: B,* vol. 69, pp. 559-563, 2000.

[13]   C. Tsai, G. Anderson, R. Thompson, and B. Wacker, "Control of silicon network structure in plasma deposition," *Journal of Non-Crystalline Solids,* vol. 114, pp. 151-153, 1989.

[14]   I. Kaiser, N. Nickel, W. Fuhs, and W. Pilz, "Hydrogen-mediated structural changes of amorphous and microcrystalline silicon," *Physical Review B,* vol. 58, pp. 1718-1721, 1998.

[15]   J. Boland and G. Parsons, "Bond selectivity in silicon film growth," *Science,* vol. 256, p. 1304, 1992.

[16]   N. Nickel and W. Jackson, "Hydrogen-mediated creation and annihilation of strain in amorphous silicon," *Physical Review B,* vol. 51, pp. 4872-4881, 1995.

[17]   H. Shirai, J. Hanna, and I. Shimizu, "Role of Atomic Hydrogen During Growth of Hydrogenated Amorphous Silicon in the¡§Chemical Annealing¡¨," *Japanese Journal of Applied Physics,* vol. 30, 1991.

[18] W. Spear and P. Comber, "Electronic properties of substitutionally doped amorphous Si and Ge," *Philosophical Magazine,* vol. 33, pp. 935-949, 1976.

[19] T. Roschek, "Microcrystalline silicon solar cells prepared by 13.56 MHz PECVD," 2003.

[20] R. Schropp and M. Zeman, *Amorphous and microcrystalline silicon solar cells: modeling, materials, and device technology*: Kluwer Academic Publishers, 1998.

[21] A. Matsuda and K. Tanaka, "Plasma Spectroscopy Glow-Discharge Deposition of Hydrogenated Amorphous-Silicon," *Thin Solid Films,* vol. 92, pp. 171-187, 1982.

[22] J. Perrin, O. Leroy, and M. C. Bordage, "Cross-sections, rate constants and transport coefficients in silane plasma chemistry," *Contributions to Plasma Physics,* vol. 36, pp. 3-49, 1996.

[23] C. Wronski and R. Collins, "Phase engineering of a-Si: H solar cells for optimized performance," *Solar Energy,* vol. 77, pp. 877-885, 2004.

[24] A. Matsuda, "Formation kinetics and control of microcrystallite in [mu] c-Si: H from glow discharge plasma," *Journal of non-crystalline Solids,* vol. 59, pp. 767-774, 1983.

[25] K. Nakamura, K. Yoshino, S. Takeoka, and I. Shimizu, "Roles of atomic hydrogen in chemical annealing," *Japanese Journal of Applied Physics,* vol. 34, pp. 442-449, 1995.

[26] A. Matsuda, "Growth mechanism of microcrystalline silicon obtained from reactive plasmas," *Thin Solid Films,* vol. 337, pp. 1-6, 1999.

[27] J. Robertson, "Growth mechanism of hydrogenated amorphous silicon," *Journal of non-crystalline Solids,* vol. 266, pp. 79-83, 2000.

[28] A. Matsuda, "Microcrystalline silicon.:: Growth and device application,"

Journal of non-crystalline Solids, vol. 338, pp. 1-12, 2004.

[29]   R. Terasa, M. Albert, H. Gruger, A. Haiduk, and A. Kottwitz, "Investigation of growth mechanisms of microcrystalline silicon in the very high frequency range," *Journal of non-crystalline Solids,* vol. 266, pp. 95-99, 2000.

[30]   R. Van Oort, M. Geerts, J. Van Den Heuvel, and J. Metselaar, "Hydrogen plasma etching of amorphous and microcrystalline silicon," *Electronics Letters,* vol. 23, p. 967, 1987.

[31]   D. Staebler and C. Wronski, "Reversible conductivity changes in discharge-produced amorphous Si," *Applied Physics Letters,* vol. 31, pp. 292-294, 1977.

[32]   M. Stutzmann, W. Jackson, and C. Tsai, "Light-induced metastable defects in hydrogenated amorphous silicon: A systematic study," *Physical Review B,* vol. 32, pp. 23-47, 1985.

[33]   A. Matsuda, M. Takai, T. Nishimoto, and M. Kondo, "Control of plasma chemistry for preparing highly stabilized amorphous silicon at high growth rate," *Solar Energy Materials and Solar Cells,* vol. 78, pp. 3-26, 2003.

[34]   M. Bennett and K. Rajan, "Stability of multijunction a Si: H based solar cells," *Journal of Applied Physics,* vol. 67, p. 4161, 1990.

[35]   S. Wieder, B. Rech, C. Beneking, F. Siebke, W. Reetz, and H. Wagner, "Influence of hydrogen dilution and substrate temperature on the initial and stabilized performance of a-Si: H solar cells," 1995, p. 234¡V237.

[36]   S. Miyajima, A. Yamada, and M. Konagai, "Highly conductive microcrystalline silicon carbide films deposited by the hot wire cell method and its application to amorphous silicon solar cells," *Thin Solid Films,* vol. 430, pp. 274-277, 2003.

[37]   J. Rath, F. Rubinelli, and R. Schropp, "Microcrystalline n-and p-layers at the

tunnel junction of a-Si: H/a-Si: H tandem cells," *Journal of non-crystalline Solids,* vol. 227, pp. 1282-1286, 1998.

[38]   J. Loffler, A. Gordijn, R. Stolk, H. Li, J. Rath, and R. Schropp, "Amorphous and micromorph silicon tandem cells with high open-circuit voltage," *Solar Energy Materials and Solar Cells,* vol. 87, pp. 251-259, 2005.

[39]   F. Rubinelli, J. Rath, and R. Schropp, "Microcrystalline nip tunnel junction in a-Si: H/a-Si: H tandem cells," *Journal of Applied Physics,* vol. 89, p. 4010, 2001.

[40]   L. Guo, M. Kondo, M. Fukawa, K. Saitoh, and A. Matsuda, "High rate deposition of microcrystalline silicon using conventional plasma-enhanced chemical vapor deposition," *JAPANESE JOURNAL OF APPLIED PHYSICS PART 2 LETTERS,* vol. 37, pp. 1116-1118, 1998.

[41]   O. Vetterl, F. Finger, R. Carius, P. Hapke, L. Houben, O. Kluth, A. Lambertz, A. Muck, B. Rech, and H. Wagner, "Intrinsic microcrystalline silicon: A new material for photovoltaics," *Solar Energy Materials and Solar Cells,* vol. 62, pp. 97-108, 2000.

[42]   J. Yang, B. Yan, and S. Guha, "Amorphous and nanocrystalline silicon-based multi-junction solar cells," *Thin Solid Films,* vol. 487, pp. 162-169, 2005.

[43]   B. Rech, T. Repmann, M. Van den Donker, M. Berginski, T. Kilper, J. Hupkes, S. Calnan, H. Stiebig, and S. Wieder, "Challenges in microcrystalline silicon based solar cell technology," *Thin Solid Films,* vol. 511, pp. 548-555, 2006.

[44]   A. Gordijn, J. Rath, and R. Schropp, "High-efficiency £gc-Si solar cells made by very high-frequency plasma-enhanced chemical vapor deposition," *Progress in Photovoltaics: Research and Applications,* vol. 14, pp. 305-311, 2006.

[45]   Y. Mai, S. Klein, R. Carius, J. Wolff, A. Lambertz, F. Finger, and X. Geng,

"Microcrystalline silicon solar cells deposited at high rates," *Journal of Applied Physics,* vol. 97, p. 114913, 2005.

[46] L. Layeillon, A. Dollet, and B. Despax, "Plasma enhanced deposition of a-Si-H: comparison of two reactor arrangements," *The Chemical Engineering Journal and The Biochemical Engineering Journal,* vol. 58, pp. 1-5, 1995.

[47] H. Caquineau and B. Despax, "Influence of the reactor design in the case of silicon nitride PECVD," *Chemical Engineering Science,* vol. 52, pp. 2901-2914, 1997.

[48] C. Raman and K. Krishnan, "A new type of secondary radiation," *Nature,* vol. 121, p. 501, 1928.

[49] D. Long, *Raman spectroscopy*: McGraw-Hill New York, 1977.

[50] R. McCreery, *Raman spectroscopy for chemical analysis*: Wiley-Interscience, 2000.

[51] M. Islam and S. Kumar, "Influence of crystallite size distribution on the micro-Raman analysis of porous Si," *Applied Physics Letters,* vol. 78, p. 715, 2001.

[52] R. Kobliska and S. Solin, "Raman spectrum of wurtzite silicon," *Physical Review B,* vol. 8, pp. 3799-3802, 1973.

[53] M. Luysberg, P. Hapke, R. Carius, and F. Finger, "Structure and growth of hydrogenated microcrystalline silicon: investigation by transmission electron microscopy and Raman spectroscopy of films grown at different plasma excitation frequencies," *Philosophical Magazine A,* vol. 75, pp. 31-47, 1997.

[54] B. Cullity, "Elements of X-ray Diffraction," *Massachusetts, USA,* 1977.

[55] S. Klein, F. Finger, R. Carius, and M. Stutzmann, "Deposition of microcrystalline silicon prepared by hot-wire chemical-vapor deposition: The influence of the deposition parameters on the material properties and solar cell

performance," *Journal of Applied Physics,* vol. 98, p. 024905, 2005.

[56]   A. Gordijn, J. Rath, and R. Schropp, "High-efficiency μc-Si solar cells made by very high-frequency plasma-enhanced chemical vapor deposition," *Progress in Photovoltaics: Research and Applications,* vol. 14, pp. 305-311, 2006.

[57]   A. Mahan, P. Raboisson, and R. Tsu, "Influence of microstructure on the photoconductivity of glow discharge deposited amorphous SiC: H and amorphous SiGe: H alloys," *Applied Physics Letters,* vol. 50, pp. 335-337, 1987.

[58]   J. Meier, S. Dubail, R. Fluckiger, D. Fischer, H. Keppner, and A. Shah, "Intrinsic Microcrystalline Silicon (c-Si: H)-A Promising New Thin Film Solar Cell Material," 1994, pp. 409-409.

[59]   M. B. v. d. Linden, J. HyvaÈrinen, W. Loyer, and R. E. I. Schropp, presented at the 13th European Photovoltaic Solar Energy Conference, 1995.

[60]   Y. Ichikawa, S. Fujikake, T. Takayama, S. Saito, H. Ota, T. Yoshida, T. Ihara, and A. Sakai, "Large-area amorphous silicon solar cells with high stabilized efficiency and their fabrication technology," 1993, pp. 27-27.

[61]   R. Arya, A. Catalano, and R. Oswald, "Amorphous silicon p i n solar cells with graded interface," *Applied Physics Letters,* vol. 49, p. 1089, 1986.

[62]   S. Guha, J. Yang, A. Pawlikiewicz, T. Glatfelter, R. Ross, and S. Ovshinsky, "Band gap profiling for improving the efficiency of amorphous silicon alloy solar cells," *Applied Physics Letters,* vol. 54, p. 2330, 1989.

[63]   M. Van den Donker, R. Schmitz, W. Appenzeller, B. Rech, W. Kessels, and M. Van de Sanden, "The role of plasma induced substrate heating during high rate deposition of microcrystalline silicon solar cells," *Thin Solid Films,* vol. 511, pp. 562-566, 2006.

[64]   O. Vetterl, A. Dasgupta, A. Lambertz, H. Stiebig, F. Finger, and H. Wagner, "Preparation Temperature Effects in Microcrystalline Silicon Thin Film Solar Cells," 2001, pp. 25-25.

[65]   Y. Nasuno, M. Kondo, A. Matsuda, H. Fukuhori, and Y. Kanemitsu, "Formation of interface defects by enhanced impurity diffusion in microcrystalline silicon solar cells," *Applied Physics Letters,* vol. 81, pp. 3155-3157, 2002.

[66]   B. Chapman, "Glow Discharge Processes Wiley," *New York,* 1980.

[67]   M. Klick, L. Eichhorn, W. Rehak, M. Kammeyer, and H. Mischke, "Influence of excitation frequency on plasma parameters and etching characteristics of radio-frequency discharges," *Surface and Coatings Technology,* vol. 116, pp. 468-471, 1999.

[68]   M. Heintze, "Versatile high rate plasma deposition and processing with very high frequency excitation," 1997.

[69]   E. Vallat-Sauvain, U. Kroll, J. Meier, A. Shah, and J. Pohl, "Evolution of the microstructure in microcrystalline silicon prepared by very high frequency glow-discharge using hydrogen dilution," *Journal of Applied Physics,* vol. 87, p. 3137, 2000.

[70]   H. Keppner, J. Meier, P. Torres, D. Fischer, and A. Shah, "Microcrystalline silicon and micromorph tandem solar cells," *Applied Physics A: Materials Science & Processing,* vol. 69, pp. 169-177, 1999.

[71]   R. Bergmann, "Crystalline Si thin-film solar cells: a review," *Applied Physics A: Materials Science & Processing,* vol. 69, pp. 187-194, 1999.